

Doctoral Dissertation

**Estimation of Upper Limb Motion Based on
Skin Deformation Measured with
a Distance Sensor Array**

Sung-Gwi Cho

March 13, 2020

Graduate School of Information Science
Nara Institute of Science and Technology

A Doctoral Dissertation
submitted to Graduate School of Information Science,
Nara Institute of Science and Technology
in partial fulfillment of the requirements for the degree of
Doctor of ENGINEERING

Sung-Gwi Cho

Thesis Committee:

Professor Tsukasa Ogasawara	(Supervisor)
Professor Yoshinobu Sato	(Co-supervisor)
Associate Professor Jun Takamatsu	(Co-supervisor)
Visiting Associate Professor Ming Ding	(Co-supervisor)
Associate Professor Masahiro Yoshikawa	(Osaka Institute of Technology)

Estimation of Upper Limb Motion Based on Skin Deformation Measured with a Distance Sensor Array*

Sung-Gwi Cho

Abstract

Upper limb motions have strong relationships with our daily life. We manipulate and grasp various daily life objects by using our upper limb. Many studies on upper limb motion estimation for human-robot and human-computer interactions have been conducted and provide important knowledge for the design of input interfaces in virtual reality and robotic applications, as well as for hand motion measurement in the medical, welfare, sporting, and manufacturing fields.

In our research, we focus on estimation of upper limb motions using skin deformation. Skin deformation is caused by the activities of various body tissues such as the muscles, tendons, and bones related to the motions. Especially, we can observe the activities of the deep layer muscles from the skin deformation.

In this dissertation, we propose estimation methods of upper limb motion based on the skin deformation. Two types of sensing devices are developed to measure the whole circumference of the skin deformation on the forearm and upper arm. We develop two categories of the motion estimation. In the first category, we develop a motion recognition method based on forearm deformation. The recognition method classifies seven different types of motions including the motions caused by the activities of deep layer muscles. In the second category, we develop two pose estimation methods. One method uses the forearm deformation and the other uses the upper arm deformation. These pose estimation method estimates multiple joint angles of the upper limb.

*Doctoral Dissertation, Graduate School of Information Science, Nara Institute of Science and Technology, March 13, 2020.

In the experiments of the motion recognition method based on the forearm deformation, we confirmed that our proposed method could recognize seven different types of hand motions including the motions related to the activities of not only surface layer muscles but also deep layer muscles. In the experiments of the pose estimation based on the forearm deformation, we confirmed that our proposed method could estimate multiple joint angles of the upper limb pose. In the experiments of the pose estimation based on the upper-arm deformation, we also confirmed that the forearm pose estimation is possible by using only upper arm deformation. These results of the experiments demonstrate that the skin deformation is useful for the upper limb motion estimation.

Keywords:

Skin deformation, distance sensor array, motion estimation/recognition, machine learning, human-machine interface

距離センサアレイを用いて計測した皮膚形状変化 に基づく上肢の動作推定*

趙 崇貴

内容梗概

上肢動作は我々の日常生活と深い関わりを持つ。我々は上肢を用いることにより、様々な日常物体の把持・操作を実現している。そのため、これまでに様々な上肢動作推定手法が開発され、VRやロボットアプリケーションの入力インタフェースや、医療福祉、スポーツ、工業分野における動作計測に応用されている。

様々な信号が上肢動作推定の入力信号として用いられるなか、我々は皮膚形状変化に着目した。皮膚形状変化は上肢の動作に関与する筋肉、腱、骨などの体組織の運動情報を反映しており、特に既存の生体信号では計測が困難な深層筋の活動を取得することができる。

本論文では、皮膚形状変化に基づく上肢の動作推定手法を提案する。はじめに、前腕と上腕の全周における皮膚形状変化を計測すべく、計測部位ごとに適した距離センサアレイを開発する。次に、様々なアプリケーションに対応すべく、動作認識と姿勢推定の2種類の手法を開発する。動作認識手法では、前腕における皮膚形状変化に基づいて深層筋の活動に関与する動作を含む7種類の手の動作を分類する。姿勢推定手法では、前腕における皮膚形状変化に基づいて前腕、手、指の姿勢を推定する。また、上腕における皮膚形状変化に基づいて、前腕の姿勢を推定する。

手の動作の認識実験では、前腕形状に基づき深層筋の活動に関与する動作を含む7種類の動作を分類可能であることを確認した。上肢の姿勢推定実験では、前腕形状に基づき前腕、手、指の姿勢を連続的に推定可能であることを確認した。また、上腕形状変化に基づき前腕の姿勢を連続的に推定可能であることを確認した。これらの実験の結果、上肢動作推定における皮膚形状変化の有用性を確認した。

*奈良先端科学技術大学院大学 情報科学研究科 博士論文, 2020年3月13日.

キーワード

皮膚形状変化, 距離センサアレイ, 動作推定・認識, 機械学習, ヒューマンマシンインタフェース

Contents

1	Introduction	2
1.1	Background	2
1.2	Skin Deformation	3
1.3	Research Objective	6
1.4	Contribution	8
1.5	Outline	9
2	Measurement Method of Skin Deformation	10
2.1	Distance Sensor Unit	10
2.2	Distance Sensor Array	12
2.2.1	Forearm Deformation	12
2.2.2	Upper Arm Deformation	14
3	Hand Motion Recognition Based on Forearm Deformation	16
3.1	Method	16
3.1.1	Overview	16
3.1.2	Measurement Setup	18
3.1.3	Feature Extraction	19
3.1.4	Generation of Training Data	19
3.1.5	Learning & Classification	22
3.2	Experiments	24
3.2.1	Experiment 1: Various users	25
3.2.2	Experiment 2: Different elbow posture	30
3.2.3	Experiment 3: Over clothing	35
3.3	Discussion	37
4	Estimation of Upper Limb Pose Based on Forearm Deformation	39
4.1	Hand Joint Angle	40
4.1.1	Method Overview	40
4.1.2	Signal Measurement & Feature Extraction	41
4.1.3	Joint Angle Regression by SVR	43

4.1.4	Experiments	44
4.2	Upper Limb Pose	47
4.2.1	Method Overview	47
4.2.2	Signal Measurement & Feature Extraction	48
4.2.3	Upper Limb Pose Estimation by DNN	52
4.2.4	Experiments	53
4.3	Discussion	67
5	Forearm Pose Estimation Based on Upper Arm Deformation	68
5.1	Method	68
5.1.1	Signal Measurement & Feature Extraction	69
5.1.2	Forearm Pose Estimation by DNN	71
5.2	Experiments	72
5.2.1	Conditions	72
5.2.2	Results	74
5.3	Discussion	77
6	Analysis and Discussion	78
6.1	Comparison Between the Skin Deformation and the sEMG	78
6.2	Potential Applications	83
7	Conclusion	86
7.1	Summary	86
7.2	Future Work	88
	Publication list	89
	References	91
	Acknowledgements	99

List of Figures

1	Radius and ulna bones displacement during pronation and supination of the forearm measured with an MRI	4
2	Cross-section of the forearm (hand side view)	5
3	Cross-section of the upper arm (elbow side view)	5
4	Required method on the estimation of upper-limb motion	8
5	Structure of the distance sensor unit	11
6	Relationship between the voltage and the distance	11
7	Position setting of the ten distance sensor units (hand side view) .	13
8	Position setting of the eight distance sensor units (elbow side view)	15
9	Procedure of the hand motion recognition	17
10	Measurement setup for the hand motion recognition	18
11	Motions of the robot hand shown on a display	20
12	An example of the feature vector and labeling result	21
13	Structure of the deep neural network for the hand motion recognition	23
14	Accuracy of recognizing hand motion in each classifier	27
15	Confusion matrix of each classifier for all subjects [%]	28
16	Tested elbow postures	31
17	Accuracy of each elbow posture in scenario 1 [%]	33
18	Accuracy of each elbow posture in scenario 2	34
19	Measurement conditions	35
20	Accuracy of each measurement condition	36
21	Overview of the estimation of hand joint angle	40
22	The measurement setup for the estimation of the hand joint angle	42
23	Flow of the estimation	43
24	An example of the results of the hand joint angle estimation . . .	46
25	Overview of the upper limb pose estimation	47
26	Measurement setup for the upper limb pose estimation	48
27	APR of each channel with upper limb motions	50
28	An example of the acquired angles	51
29	Structure of the network for the upper limb pose estimation . . .	52
30	Guide motions of a robot arm	55

31	An example of the estimated and target poses in the experiment 1	57
32	RMSE of each axis in the experiment 1	58
33	RMSE in the moving range of each axis in the experiment 1 . . .	59
34	An example of the estimated and target poses with BVH viewer in the experiment 1	60
35	Target motions in the experiment 2	61
36	An example of the estimated and target poses in the experiment 2	63
37	RMSE of each axis in the experiment 2	64
38	RMSE in the moving range of each axis in the experiment 2 . . .	65
39	An example of the estimated and target poses with BVH viewer in the experiment 2	66
40	Overview of the forearm pose estimation	68
41	Measurement setup for the forearm pose estimation	69
42	An example of the feature vector and the forearm poses	70
43	Architecture of the model for the forearm pose estimation	71
44	Measured motion conditions	73
45	Estimation results on the condition 1	75
46	Estimation results on the condition 2	76
47	Forearm deformation measured with the developed distance sensor array in the poses of wrist extension and radial flexion	80
48	Forearm deformation measured with the distance sensor array and cross-section measured with an MRI in the pose of pronation and supination	81

List of Tables

1	Relationship between measurement part and estimated motion/pose	8
2	Accuracy of hand motion recognition with DNN [%]	29
3	RMSE for each subject on the hand joint angle estimation	45
4	RMSE for each subject on the forearm pose estimation	74
5	Functions of the forearm muscles	79
6	Functions of the upper arm muscles	79
7	Differences between the sEGM and skin deformation	82

Chapter 1

Introduction

1.1 Background

Upper limb motions have strong relationships with our daily life. We manipulate and grasp various daily life objects by using our upper limb. Many studies on estimation of upper limb motion for human-robot and human-computer interactions have been conducted and provide important knowledge for the design of input interfaces in virtual reality and robotic applications [1–7], as well as for hand motion measurement in the medical, welfare, sporting, and manufacturing fields and daily life [8–12].

To accurately estimate the motions, various input information has been used such as visual, inertial and magnetic information, and bio-signals. The first one is visual information [13–17]. RGB and/or RGB-D cameras can acquire the contour and appearance of the hand. By using a machine-learning-based method such as a Convolutional Neural Network (CNN) [18], the upper limb motion is accurately estimated [19, 20]. Simon *et al.* [13] estimated 3D hand pose based on a single RGB image using multiview bootstrapping. The visual-based method is effective when the hand is not perfectly occluded by the objects or when multiple cameras can be placed in the measurement environment.

The second one is information from the Inertial Measurement Unit (IMU) sensors and magnetic sensors [21–26]. They are directly attached to the hands to measure the hand pose. Kortier *et al.* [21] attached the IMU and magnetic sensor on fingers and tracked independent finger poses. The IMU and magnetic sensor-based methods are effective when the sensors can be attached directly to the hand.

The third one is information from bio-signals such as a surface electromyogram (sEMG) [5–7, 27–34]. These bio-signals are directly related to the hand or elbow motions since these can include information about muscle activities. In addition to the sEMG, a force myogram (FMG) is widely used. By using the

FMG measured with a force sensor [35–38] or an air-pressure sensor [39], the force distribution between the skin and a fixture can be obtained. In addition, various other signals are also used such as bend information [40], an ultrasound [41, 42] and a bone sound [43]. In these methods, machine-learning-based methods have been proposed to estimate hand motions by analyzing the measured bio-signals. Yoshikawa *et al.* [27] recognized seven different hand motions based on the sEMG using Support Vector Machine. Shima *et al.* [28] recognized combined hand motions based on the sEMG using Recurrent Log-Linearized Gaussian Mixture Network. The bio-signal based method is effective when the measurement environment and conditions are not fixed because the signal can be measured using a wearable sensor that is attached on the part of the body except for the hand. Thus, the methods based on the bio-signals have gained popularity.

1.2 Skin Deformation

In our research, we focus on the estimation of upper limb motions using skin deformation. The reason why we chose the skin deformation is that the activities of surface and deep layer muscles, tendons, and bones can be extracted from the skin deformation in a non-invasive manner. The skin shape is changed with the body tissues related to upper limb motions. Especially, we can observe the activities of the deep layer muscles from the skin deformation which is difficult to observe from the sEMG.

To measure skin deformation, an optical sensor is often used. Makino *et al.* [44] proposed a tangential force sensing system on the forearm using the photo reflective sensors. Ogata *et al.* [45] proposed a skin gesture interaction system using the photo reflective sensors. Oka *et al.* [46] developed a photo reflective sensors array to measure muscle activity. Unlike the FMG-based method, by using the optical sensor, skin deformation can be measured without the fixture which is closely matched on the body part.

In previous methods for estimation of upper limb motion based on the skin deformation, Fukui *et al.* [47] proposed a finger motion recognition method using a wrist contour measuring device. Sugiura *et al.* [48] measured the deformation on the back of the hand and recognized finger motions. These studies mainly measure the activities of the tendons which related to finger motions. Kato *et*

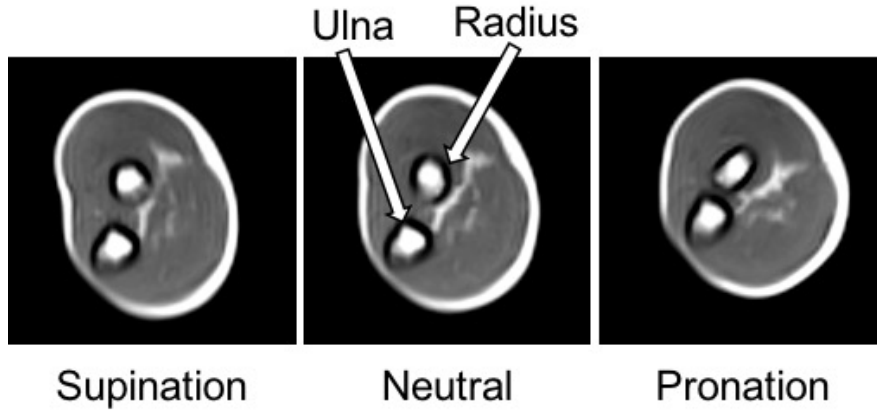


Fig. 1. Radius and ulna bones displacement during pronation and supination of the forearm measured with an MRI

al. [49] measured the muscle bulge movement along the longitudinal direction of the forearm and estimated the wrist joint angle using an array of distance sensors. Previous studies showed that to measure skin deformation near the hand for estimating finger motions and to measure skin deformation along the forearm in the longitudinal direction for estimating hand motions are effective.

On the other hand, skin deformation on the forearm where position close to the elbow contains rich information from various muscle activities and bone movements. In the forearm, the round pronator and the supinator muscles are deep layer muscles and related to the forearm pronation and supination. When the forearm is pronated and supinated, not only muscles but also bones are moved, as shown in Fig. 1. By the deformation of the muscles and tendons and the displacement of the bones, the shape of the skin is characteristically changed with various upper limb motions including the motions related to the activities of the deep layer muscles. Moreover, the forearm deformation provides the motions of not only the forearm and hand but also the finger. In the forearm, the flexor digitorum superficialis, flexor digitorum profundus, extensor digitorum communis, and flexor pollicis longus muscles are related to finger motions. The deformation related to finger motions also could be observed on the forearm position closed to the elbow.

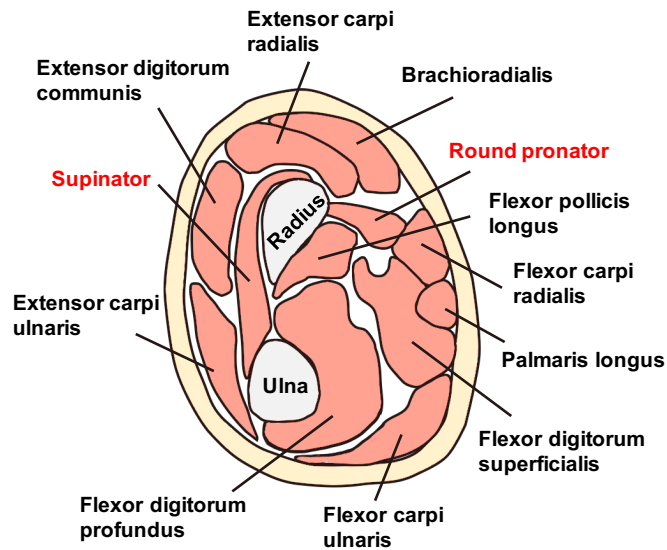


Fig. 2. Cross-section of the forearm (hand side view)

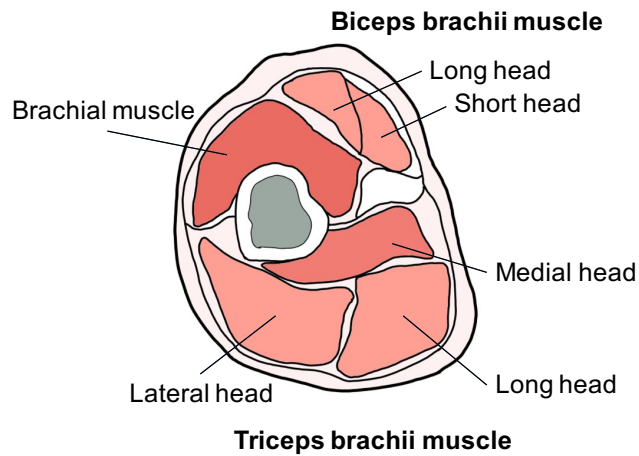


Fig. 3. Cross-section of the upper arm (elbow side view)

Fig. 2 shows the cross-section of the forearm. There are many muscles related to upper limb motions are involved. In order to measure the activities of various muscles, it is necessary to measure the whole circumference of the measurement part. If it becomes possible to measure the deformation of the entire region with high accuracy, various upper limb motions can be estimated.

Moreover, skin deformation on the upper arm also has rich information to estimate upper limb motions. Fig. 3 shows the cross-section of the upper arm. The number of the muscles is few comparing with the forearm. The main muscles in the upper arm are the biceps brachii and triceps brachii. The main function of both muscles is the elbow flexion and extension. On the other hand, the biceps brachii muscle also contributes to supinate the forearm when the elbow is flexed. Therefore, the shape of the upper arm is changed not only the elbow flexion and extension but also the forearm pronation and supination. The forearm poses are decided by joint angles of both the elbow flexion and extension but also the forearm pronation and supination. If it becomes possible to measure the deformation on the upper arm, the forearm pose can be estimated.

In both of forearm and upper arm, we aim to estimate the motions of digital parts from the measurement position. To measure the input signal on the digital position from target body parts and estimate the motions, we can provide a variety of sensor attachment positions.

1.3 Research Objective

In this dissertation, we propose estimation methods of upper-limb motions based on the skin deformation on the forearm or upper arm (forearm deformation and upper arm deformation). We measure the whole circumference of the forearm deformation and upper arm deformation using a distance sensor array. By using the measured skin deformation, we estimate various upper limb motions. To deal with various applications, we develop two categories of motion estimation, as shown in Fig. 4.

Motion recognition

In the first category, we develop a motion recognition method base on forearm deformation. The motion recognition method classifies motion classes.

For example, for the input interface of the prosthesis hand, the motion recognition method is widely used. To control axes corresponding to recognized motions, the intuitive operation is realized. Skin deformation has a possibility to recognize motions from the activities of not only the surface layer muscles but also the deep layer muscles. If the motion recognition including the motions from the activities of the deep layer muscles is possible, we can confirm the usefulness of the skin deformation.

Therefore, we propose a motion recognition method based on forearm deformation. The method recognizes seven different types of motions including pronation and supination which are targeted in the previous method based on the sEMG [27].

Pose estimation

In the second category, we develop two pose estimation methods. The studies of the pose estimation based on bio-signals are fewer than the studies of motion recognition. The degree of freedom which needs to estimate is higher than the motion recognition. For the pose estimation, the methods based on visual or inertial and magnetic sensor information are widely used. If the pose (e.g., joint angle) estimation is possible, we can confirm the usefulness of the skin deformation and expand the applied field of the method based on bio-signals. Therefore, we propose pose estimation methods based on forearm/upper-arm deformation.

The method based on the forearm deformation estimates the pose of the forearm, hand, and finger. In the method, to confirm the performance for not only interface but also motion measurement in daily life, we estimate not only simple motion but also combined motion in daily life.

The method based on the upper arm deformation estimates the pose of the forearm. When estimating the forearm pose, it is common to measure the bio-signal on the forearm. However, if the forearm pose estimation based on upper arm deformation is possible, we can remove the limitation of the sensor attached part for the various application.

Table 1 shows the relationship between the measurement part and the estimated motion/pose in this dissertation. We evaluate the performance of each

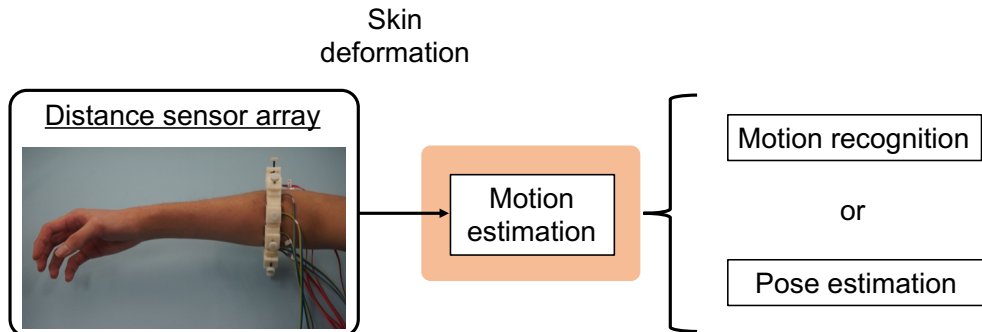


Fig. 4. Required method on the estimation of upper-limb motion

Table 1. Relationship between measurement part and estimated motion/pose

Measurement part	Types of estimation	Target motion/pose
Forearm	Motion recognition	Seven types of hand motions
	Pose estimation	Poses of forearm, hand, and finger
Upper arm	Pose estimation	Pose of forearm

method in this dissertation. This dissertation clarifies the performance of upper-limb motion estimation from skin deformation.

1.4 Contribution

The contribution of this dissertation is three-fold.

- First, we develop a measurement system of the skin deformation using a distance sensor array. Two types of distance sensor arrays are developed to measure skin deformation on the forearm and upper arm.
- Second, we propose a hand motion recognition method based on forearm deformation to recognize seven types of hand motions including the motions related to the activities of the deep layer muscles.
- Third, we propose estimation methods of upper limb pose based on the skin deformation. We estimate the upper limb pose based on forearm deformation. We also estimate forearm pose based on upper arm deformation.

1.5 Outline

The remainder of this dissertation is organized as follows.

Chapter 2 describes a measurement device of the skin deformation.

Chapter 3 describes a hand motion recognition method based on forearm deformation.

Chapter 4 describes an estimation method of the upper-limb pose based on forearm deformation.

Chapter 5 describes a forearm pose estimation method based on upper arm deformation.

Chapter 6 describes an analysis of the skin deformation and a discussion about potential applications.

Finally, chapter 7 draws the conclusion of this dissertation.

Chapter2

Measurement Method of Skin Deformation

To measure skin deformation, we develop distance sensor arrays. In this chapter, we describe the measurement method of skin deformation using the distance sensor array.

2.1 Distance Sensor Unit

To measure the deformation of the skin, we use a distance sensor array, which consists of multiple distance sensor units. The distance sensor unit is developed based on the sensor for the input interface of the electrical prosthesis hand [50]. Fig. 5 shows the structure of the distance sensor unit. The distance sensor (SG-105, Kodenshi) converts a distance to a voltage using GaAs Infrared Emitting Diodes (IRED) and a high-sensitivity phototransistor. The distance sensor unit measures the distance between the infrared-based distance sensor and the ABS resin plate. Fig. 6 shows the relationship between the distance and the output voltage. The sensor can stably measure the distance from 0.5 to 3.0 mm. The standard deviation for the output voltage of the sensor is less than 0.014 V in each 0.1 mm on ten times.

An elastically deformable sponge (PORON, Rogers Inoac) which expands and contracts in response to the forearm deformation is arranged around the distance sensor, between the sensor and the resin plate. A reflection sheet (AHW001, Waki Sangyo) is attached inside the plate to suppress noise caused by external light. This sheet helps to keep the inside dark.

Note that the sensor unit can measure deformation even over clothing, unlike sEMG sensing. The output signals of the distance sensor unit can be directly inputted to an analog-to-digital (A/D) converter without an amplifier or filter.

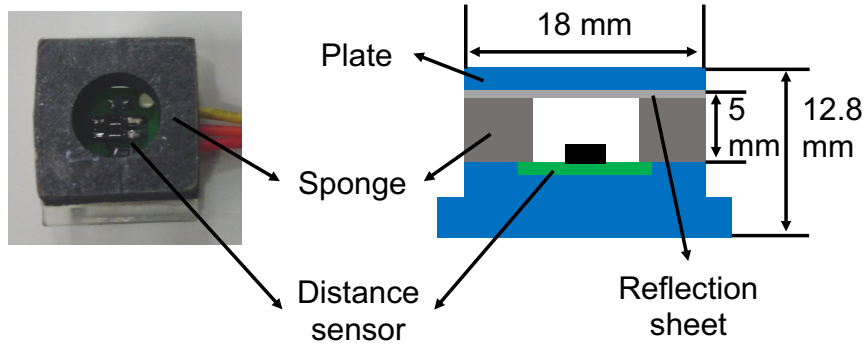


Fig. 5. Structure of the distance sensor unit

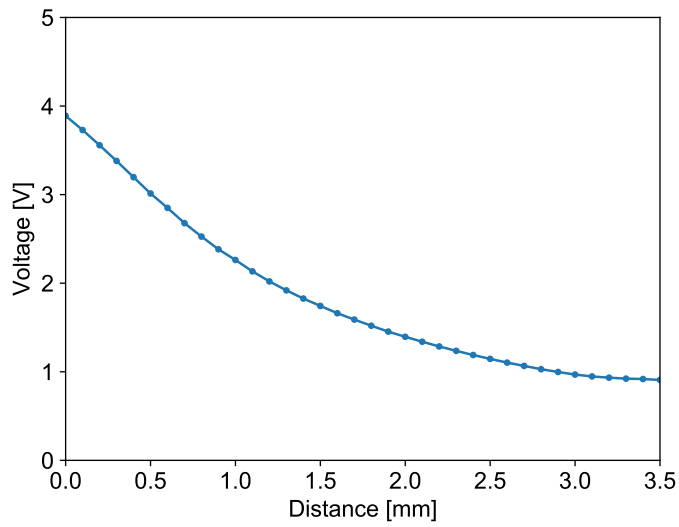


Fig. 6. Relationship between the voltage and the distance

2.2 Distance Sensor Array

We develop two types of distance sensor arrays to measure skin deformation on the forearm and upper arm. In this section, we describe the design of each array. The measured signals from the arrays and the performance for the motion estimation are discussed in chapter 3 to chapter 5.

2.2.1 Forearm Deformation

The array to measure forearm deformation has ten channels of the distance sensor units. As shown in Fig. 7, the distance sensor units are arranged following the cross-section of the forearm. The cross-section is not a perfect ellipsoid. The ulna side is wider than the radius side because thick flexors exist on the ulna side. Thus, we design the shape of the array to follow the forearm curve on the cross-section. Since the size of user's forearm varies, the amount of the distance sensor unit has a screw mechanism that allows adjusting the position of the unit to fit the user's forearm.

When the user wears the distance sensor array on the forearm, the array is set to the maximum circumference of the forearm. Moreover, Ch. 1 of the distance sensor array is set over the extensor carpi radialis. We adjust the size so that each channel sinks down at least 0.5 mm deflection in the initial pose.

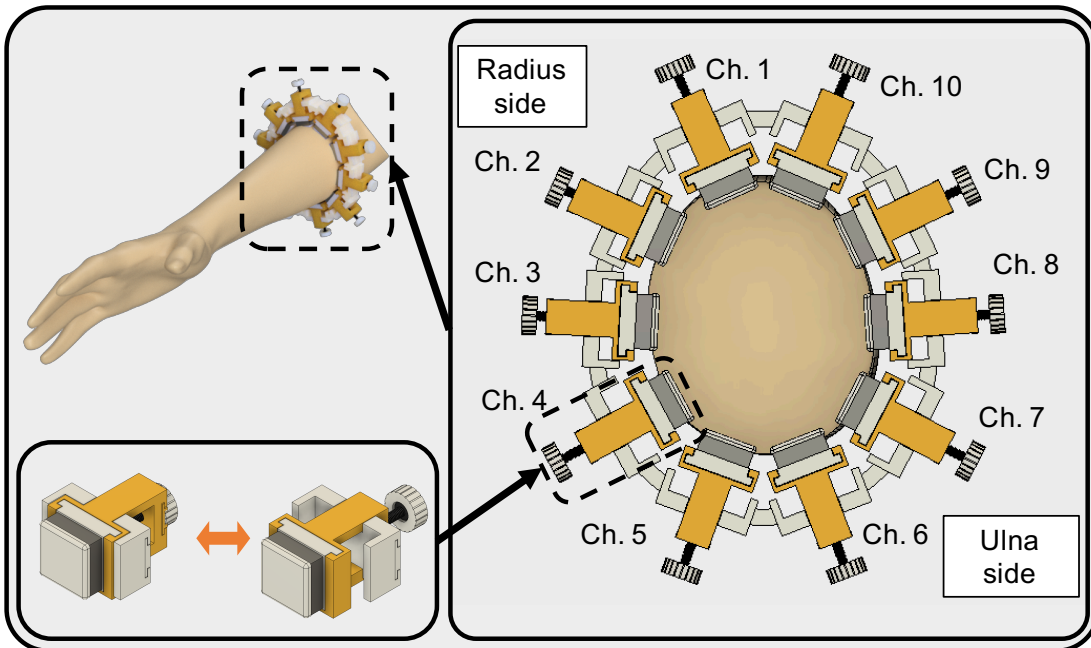


Fig. 7. Position setting of the ten distance sensor units (hand side view)

2.2.2 Upper Arm Deformation

As shown in Fig. 8, eight channels of the distance sensor units are set to measure upper arm deformation. The number of muscles in the upper arm is fewer than the forearm. Therefore, we change the number of the distance sensor units from ten to eight. We design the shape of the sensor array to fit the upper arm to arrange Ch. 1 and Ch. 5 on the biceps brachii and the triceps brachii muscles, respectively. An adjusting mechanism has also been designed to fit the size of the array for various sizes of the upper arm. Since the size of user's upper arm also varies, the amount of the distance sensor unit has a screw mechanism that allows adjusting the position of the unit to fit the user's upper arm. By changing the number of the distance sensor units, it is easy to adjust the array with various size of the upper arm.

When the user wears the distance sensor array on the upper arm, the array is adjusted to the position near the elbow on the upper arm. We attach the developed distance sensor array to the user's upper arm by setting the Ch. 1 sensor unit on the biceps brachii muscle. We adjust the size so that each channel sinks down at least 0.5 mm deflection in the initial pose.

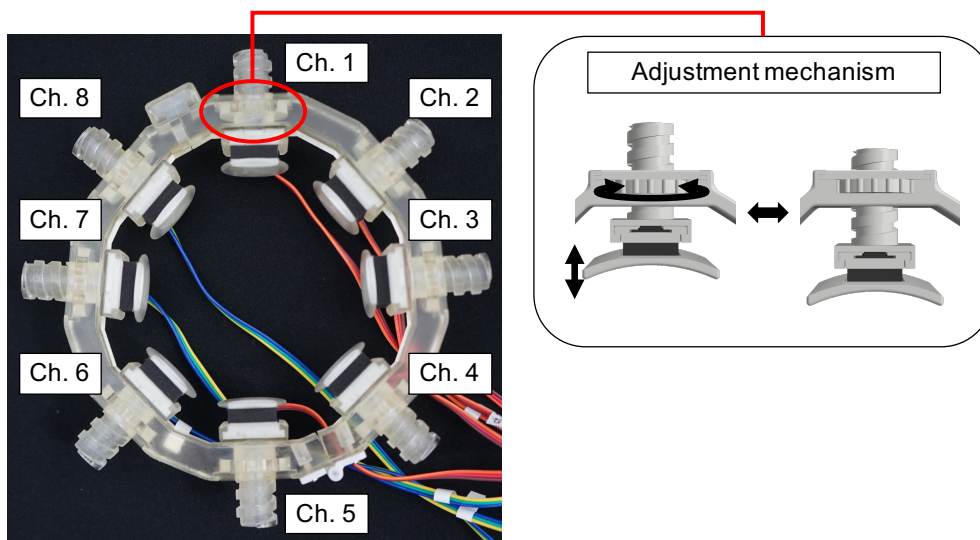


Fig. 8. Position setting of the eight distance sensor units (elbow side view)

Chapter3

Hand Motion Recognition Based on Forearm Deformation

To recognize the motions from the activities of the deep layer muscles, we propose a hand motion recognition method by measuring the forearm deformation using a distance sensor array.

3.1 Method

3.1.1 Overview

Fig. 9 shows an overview of the hand motion recognition method. We focus on recognizing seven different motions which are targeted in the previous method based on the sEMG [27]:

- NE: neutral
- WF and WE: wrist flexion and extension
- HC and HO: hand closing and opening
- PR and SU: pronation and supination of the forearm.

In the target motions, the pronation and supination of the forearm are caused by the activities of the deep layer muscles (round pronator and supinator). In the proposed method, the user's forearm deformation is measured with the distance sensor array. After measuring forearm deformation, the method recognizes hand motions. The method consists of three parts which are listed here and described below.

Feature Extraction

After measurement of the forearm deformation using the distance sensor array, a feature vector for hand motion recognition is extracted.

Generation of Training Data

The motion labels are automatically assigned to reduce the burden on the users. The method shows the instructions and timing of the hand motions for training and then the method calculates motion segments based on signal intensities and the instruction.

Learning & Classification

Finally, using extracted feature vectors and the annotated motion labels, a motion classification model is trained. After training, the method recognizes hand motions from forearm deformation.

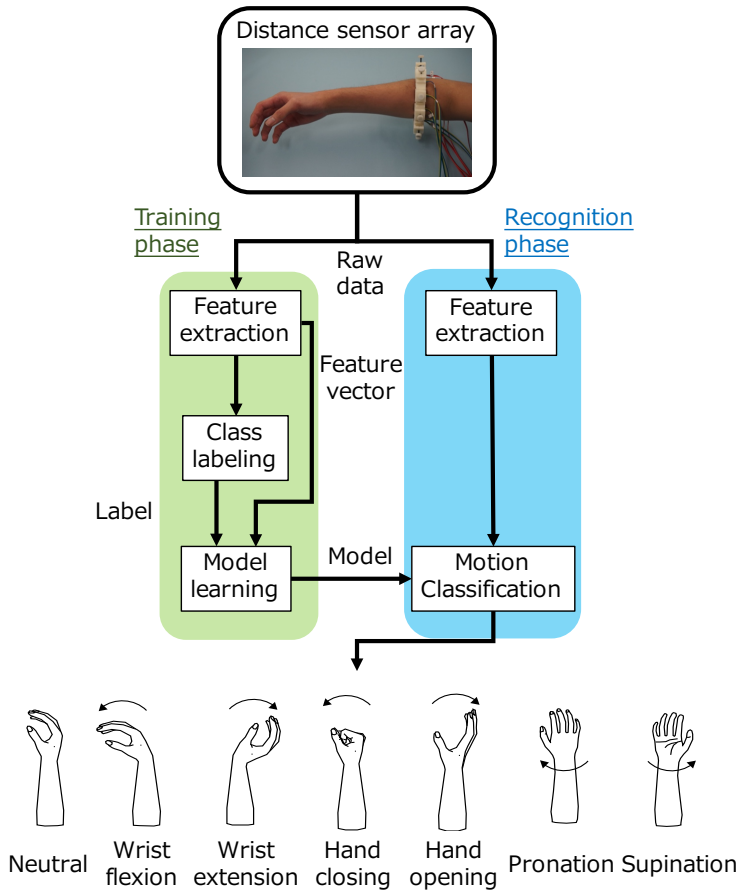


Fig. 9. Procedure of the hand motion recognition

3.1.2 Measurement Setup

Fig. 10 shows the measurement setup. A PC and an A/D converter (USB-6218, National Instruments) are connected with a USB cable. The distance sensor array, A/D converter, and a stabilized power source are also connected with cables. We adjust the size of the array so that each channel sinks down at least 0.5 mm deflection in the neutral pose. The raw data from the distance sensor array is measured using the A/D converter at a sampling rate of 2000 Hz.

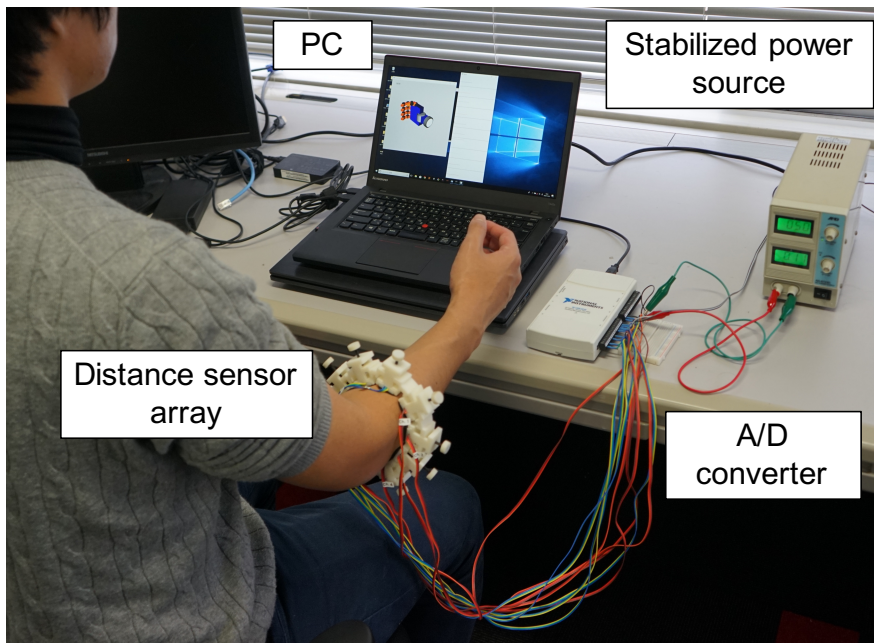


Fig. 10. Measurement setup for the hand motion recognition

3.1.3 Feature Extraction

A feature vector is extracted for each frame. The number of samples in each frame is N . We take the feature vector from 128 samples (64 ms) as one frame. The frame is shifted for 32 samples (16 ms).

In each frame, we calculate an APR feature that we proposed for hand motion recognition. The APR is the average of distance sensor data and is calculated as follows:

$$APR_l(p) = \frac{1}{N} \sum_{n=1}^N PR_l(n), \quad (1)$$

where PR_l ($n = 1, \dots, N; l = 1, \dots, L$) is the n^{th} sampled signal measured with the l^{th} channel in the p^{th} frame. In this method, the number of channels L is ten. The feature vector $\mathbf{x}(p)$ consists of the L -dimensional APR as follows:

$$\mathbf{x}(p) = (APR_1(p), \dots, APR_L(p)). \quad (2)$$

3.1.4 Generation of Training Data

Generally, collecting and annotating the training data is a key issue in the use of machine learning. The training data should have paired input data, e.g., feature vectors, and desired output, e.g., hand motion labels. The desired output must be assigned carefully considering the input data.

In the training phase, users perform seven hand motions following the displayed motions of a virtual robot hand on a display. Fig. 11 shows the motions of the robot hand which are used to guide the user's motions. For training, the users continuously perform the target motions just as in actual use. Then we extract the motion segments consisting of the same type of motions.

Since the user imitates the robot hand motions, we assume that the boundary of a segment is located near the center of the transition between the two motions. First, the APR_l is scaled and shifted with $\min = 0$ and $\max = 1$ for each channel. Second, we calculate the displacement of the APR of each channel (APR_l^{disp}) using the following equation:

$$APR_l^{disp}(p) = \|APR_l(p) - APR^{NE}\|, \quad (3)$$

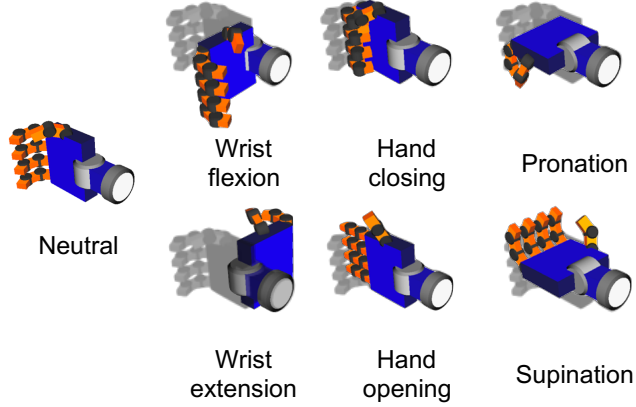


Fig. 11. Motions of the robot hand shown on a display

where APR^{NE} is an average of APR in the segments where the robot hand is fixed in the neutral posture. Third, APR_c^{disp} of a characteristic signal is searched using the following equation:

$$c = \arg \max_{1 \leq l \leq L} APR_l^{disp}. \quad (4)$$

Finally, the actual motion segment is determined between the $\max APR_c^{disp}$ and $\max APR_c^{disp} \times Th$. In this study, we use $Th = 0.5$. Since we assume there is a correlation between the hand motions and the forearm deformation, we take 50% from the peak for the operation segments.

Fig. 12 shows an example of the feature vector (10-dimensional APR) and the calculated motion labels. For each motion, the motion labels are determined for the motion segments and characteristic signals can then be observed in each channel.

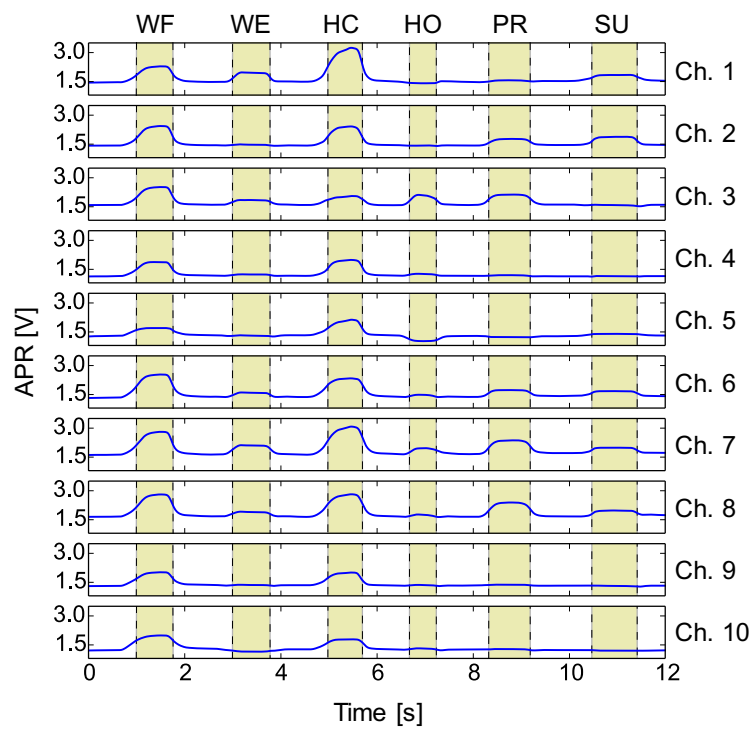


Fig. 12. An example of the feature vector and labeling result

3.1.5 Learning & Classification

To select an optimal classifier for hand motion recognition based on forearm deformation, we test three types of classifiers which are often used: k-Nearest Neighbor (k-NN) [51], Support Vector Machine (SVM) [52], and Deep Neural Network (DNN) [53].

k-Nearest Neighbor (k-NN) k-NN classifies classes based on the number of near samples in the input data. In our study, the best number of k , which is a parameter of k-NN, is decided from five patterns ($k \in \{1, 3, 5, 7, 9\}$).

Support Vector Machine (SVM) In SVM, the decision function for classifying the feature vector \mathbf{x} is expressed as:

$$f(\mathbf{x}) = \text{sign}\left(\sum_{i=1}^D \lambda_i y_i K(\mathbf{x}_i, \mathbf{x}) + b\right), \quad (5)$$

where y_i is a binary class label corresponding to the i^{th} training sample \mathbf{x}_i . D is the number of training samples, λ_i is a Lagrange multiplier, and b is a bias. $K(\mathbf{x}_i, \mathbf{x})$ is a kernel function. In our study, a radial basis function (RBF) kernel is used as the kernel function K :

$$K(\mathbf{x}_i, \mathbf{x}) = \exp(-\gamma \|\mathbf{x}_i - \mathbf{x}\|^2), \quad (6)$$

where γ is a kernel parameter.

To apply the SVM to multiple class classification problems, we use the one-versus-one method. In this case, SVM classifies classes using $O(O-1)/2$ decision functions, where O is the number of classes.

The best combination of hyperparameters is decided by a grid search. There are 56 pattern combinations for the kernel parameter $\gamma \in \{2^{-5}, 2^{-4}, \dots, 2^1\}$ and the penalty $C \in \{2^1, 2^2, \dots, 2^8\}$. C is a parameter of the margin.

Deep Neural Network (DNN) We use a fully-connected multiple-layer deep neural network. As shown in Fig. 13, our network consisted of an input layer, an output layer, and five hidden layers. The number of the input nodes is ten. The

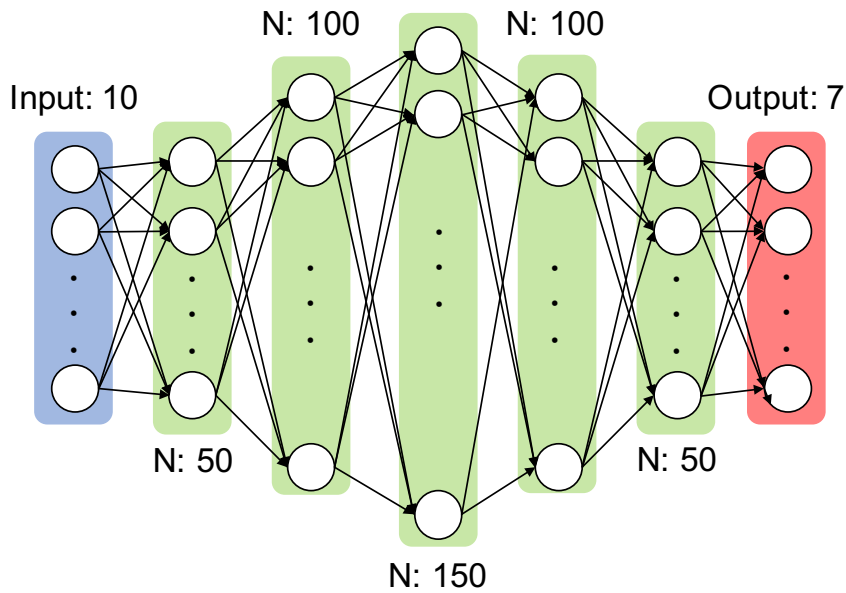


Fig. 13. Structure of the deep neural network for the hand motion recognition

number of the output nodes is seven. The numbers of the nodes of each hidden layer are 50, 100, 150, 100, and 50. A ReLU is used as the activation function of the hidden layers. The activation function of the output layer is a softmax. The structure of the network is experimentally determined.

We use an Adam [54] as the optimizer and a categorical cross-entropy as the loss function. The model is trained with a batch size of 1000 and 100 epochs.

3.2 Experiments

We describe the conditions and results of the hand motion recognition experiments with the proposed method. We performed three types of hand motion recognition experiments.

Experiment 1: Various users

For various applications, the method needs to recognize hand motions of various users. We verified the accuracy of the proposed method with nine different subjects.

Experiment 2: Different elbow posture

The shape of the forearm changes not only with hand motions but also with elbow postures. We verified the accuracy of hand motion recognition with three types of different elbow posture.

Experiment 3: Over clothing

Our distance sensor array can measure forearm deformation over clothing. We verified the accuracy by comparing direct measurement and measurement over clothing.

The experimental protocol was approved by the research ethics board of the Nara Institute of Science and Technology. Before participation in the experiments, informed consent was obtained from the subjects.

3.2.1 Experiment 1: Various users

Conditions We performed this experiment with nine healthy subjects A to I with the following characteristics:

- Age: eight in their 20’s, one in 40’s
- Gender: eight males, one female
- Dominant arm: eight right-handed, one left-handed.

For this experiment, the subject wearing the distance sensor array was asked to keep their elbow posture at almost 90-degree flexion and perform seven different types of hand motions during 60 seconds as one trial. The array was attached to the subject’s dominant arm. The subject repeats neutral and the other six hand motions. Hand motions were performed in the order of wrist flexion, wrist extension, hand closing, hand opening, pronation, and supination. Each motion was performed to the maximum angle in the movable range, and then returned to the neutral position in about one second. Each trial conducted in five sets of six motions. Each subject performed ten trials.

For each subject, the data from the ten trials was tested using five-fold cross-validation. The feature vectors were then scaled and shifted as mean = 0 and variance = 1. The number of frames for each trial data was 3747. We used the frames from eight trials for training (29976 frames) and the frames from the remaining two trials for testing data (7494 frames).

The accuracy of recognition of each motion was calculated by the following equation:

$$\text{Accuracy (\%)} = \frac{\text{number of correct frames}}{\text{total number of frames}} \times 100. \quad (7)$$

Results Fig. 14 shows the accuracy of each hand motion with each classifier. Except for neutral, with each classifier, the accuracy of recognition of hand motions was 98% or more. Note that the accuracy of recognition of pronation and supination, which are related to the activities of the deep layer muscles, was also high. These results show that our method can recognize hand motions caused by the activities of both the surface layer and deep layer muscles.

For more detailed analysis, Fig. 15 shows the confusion matrix for each of the three classifiers. With the classifiers, the recognition error between the target motion and other classes was only 2% or less.

In regard to the adaptability of the method for various users, Table 2 shows the accuracy of recognition of the seven different hand motions for each subject using the DNN classifier. There were no large differences in the accuracy of recognition among the different users, and a high level of accuracy was maintained for all users.

In this experiment, there were no large differences in the accuracy among the three classifiers. However, the accuracy of recognizing the neutral was higher with the DNN classifier than with the other classifiers. This indicates that the DNN classifier can improve the recognition of the neutral.

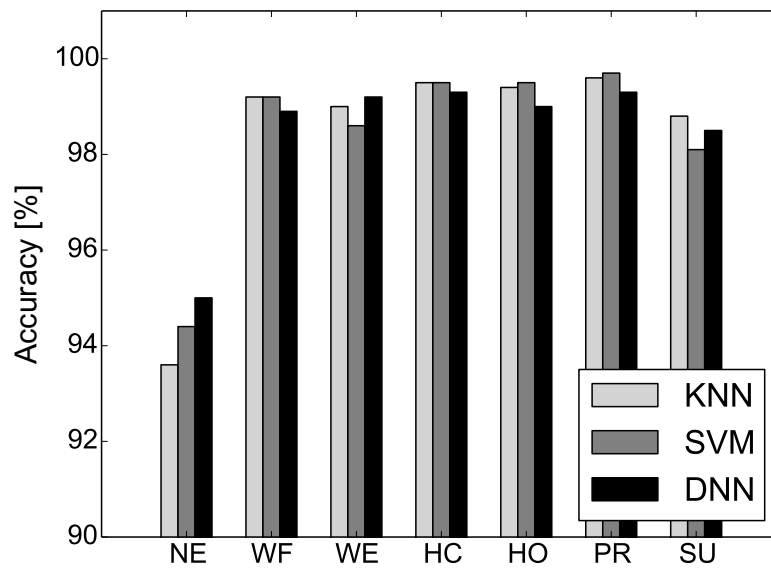
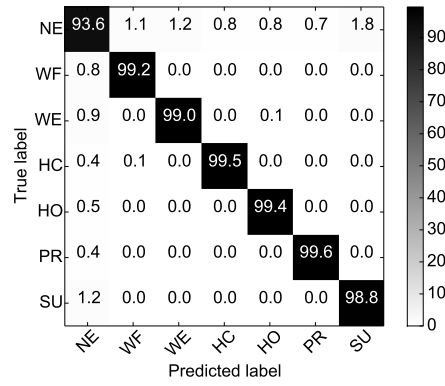
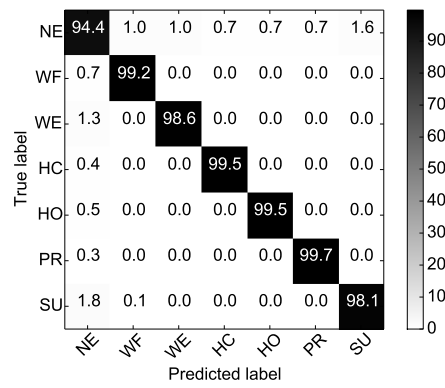


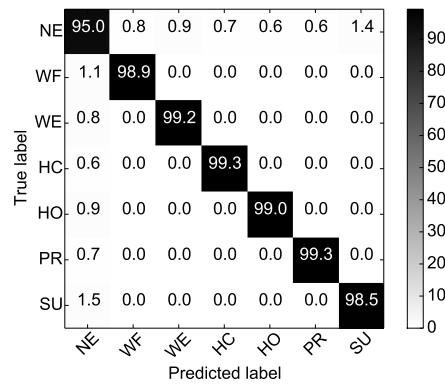
Fig. 14. Accuracy of recognizing hand motion in each classifier



(a) k-NN



(b) SVM



(c) DNN

Fig. 15. Confusion matrix of each classifier for all subjects [%]

Table 2. Accuracy of hand motion recognition with DNN [%]

ID	NE	WF	WE	HC	HO	PR	SU
A	96.1	99.7	99.8	99.2	99.7	99.3	99.9
B	96.0	99.2	98.9	99.4	99.4	97.9	99.7
C	93.8	99.2	96.8	98.9	98.6	99.7	96.9
D	97.3	98.0	99.4	99.1	99.4	99.7	99.3
E	92.6	98.6	98.9	99.7	99.4	99.6	98.0
F	94.0	99.0	99.0	99.5	97.8	99.2	97.7
G	94.5	96.4	99.6	98.9	97.8	99.6	97.9
H	95.8	99.7	99.6	99.7	99.6	99.7	99.2
I	95.2	99.2	99.6	99.5	99.3	99.3	98.0
Mean	95.0	98.9	99.2	99.3	99.0	99.3	98.5

3.2.2 Experiment 2: Different elbow posture

Conditions In this experiment, three subjects (the 20's, male, right-handed) performed five trials of hand motions with three different types of the elbow postures: flexion, middle, and extension, as shown in Fig. 16. To test the accuracy for the different training conditions, we tested the two following scenarios:

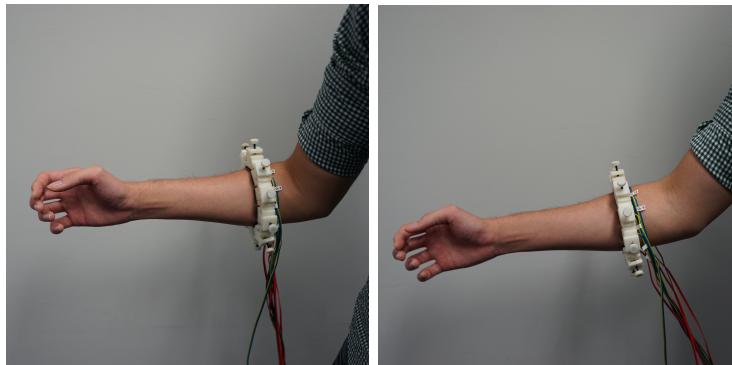
Scenario 1

The classifiers were trained using one type of elbow posture and data from four trials. Data from one trial of the hand motions for all the three types of elbow postures were then tested with the classifiers.

Scenario 2

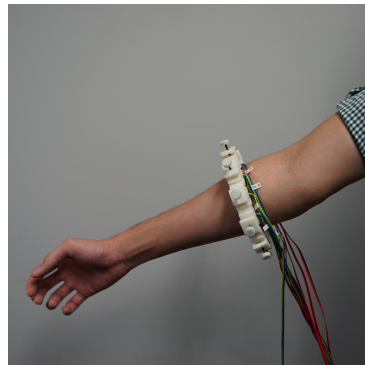
The classifiers were trained using four trials with all three types of elbow postures (12 trials of data from four trials by three types of elbow postures). Data from one trial of the hand motions with all three types of elbow postures were then tested with the classifiers.

In both scenarios, the performance of classifiers was tested using five-fold cross-validation.



(a) Flexion

(b) Middle



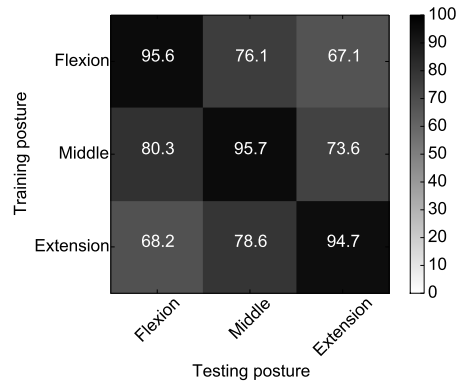
(c) Extension

Fig. 16. Tested elbow postures

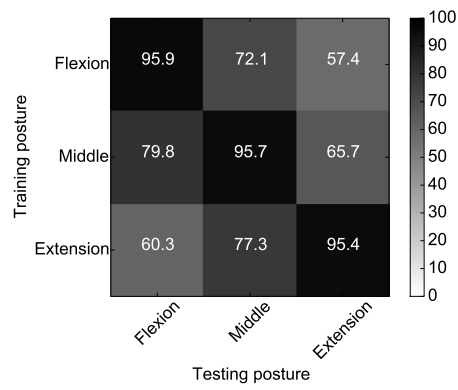
Results Fig. 17 shows the total accuracy of each classifier for each elbow posture with scenario 1. For all the classifiers, when the elbow posture was the same between the training and testing data, the accuracy was 94% or more. However, when the elbow posture was different between the training and testing data, the accuracy decreased. Specifically, the accuracy was less between extension and flexion.

Fig. 18 shows the total accuracy of each classifier for each elbow posture with scenario 2. In this scenario, with all of the elbow postures, accuracy was 94% or higher. In particular, the accuracy of the DNN classifier was higher.

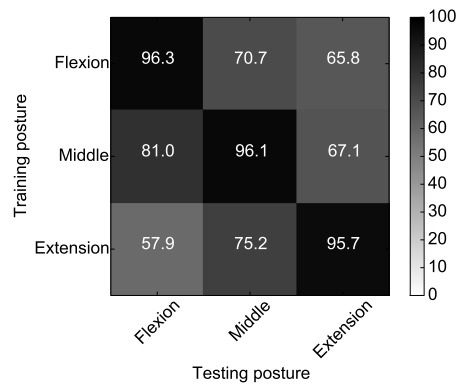
In summary, all the classifiers achieved 94% or higher accuracy in recognizing hand motions with various elbow postures using training data with various elbow postures. If the elbow posture of the hand motions is known, we can maintain this high accuracy even if the training data is limited by the target posture.



(a) k-NN



(b) SVM



(c) DNN

Fig. 17. Accuracy of each elbow posture in scenario 1 [%]

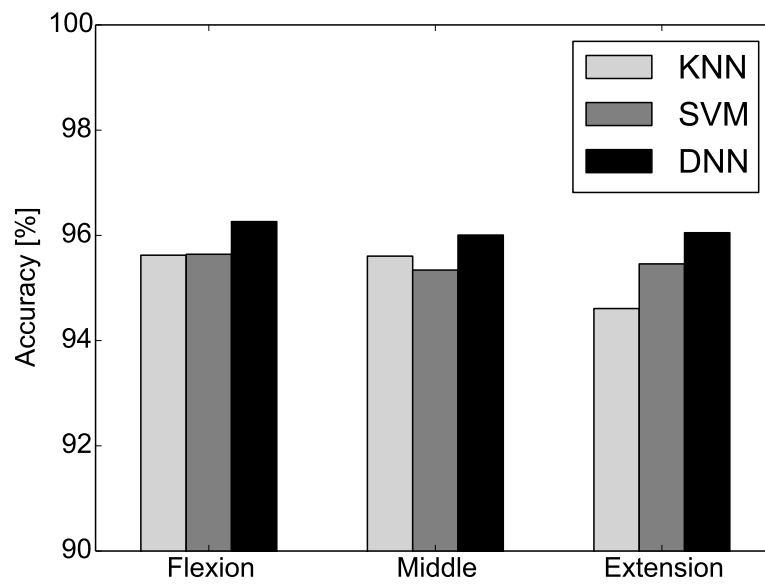


Fig. 18. Accuracy of each elbow posture in scenario 2

3.2.3 Experiment 3: Over clothing

Conditions In this experiment, three subjects (the 20's, male, right-handed) performed five trials of hand motions with two types of measurements, as shown in Fig. 19, both direct and over clothing. All three subjects wore a shirt whose thickness was about 0.5 mm. The data were tested using five-fold cross-validation.

Results Fig. 20 shows the accuracy of hand motion recognition of all three classifiers with the data from the two conditions. With both conditions, the total accuracy of the hand motions was 95% or more for all classifiers. There was no large difference in the accuracy between the two conditions. Again, the accuracy of the DNN classifier was higher than the other classifiers under both conditions. These results show that the method can recognize hand motions through both direct measurement and measurement over clothing.

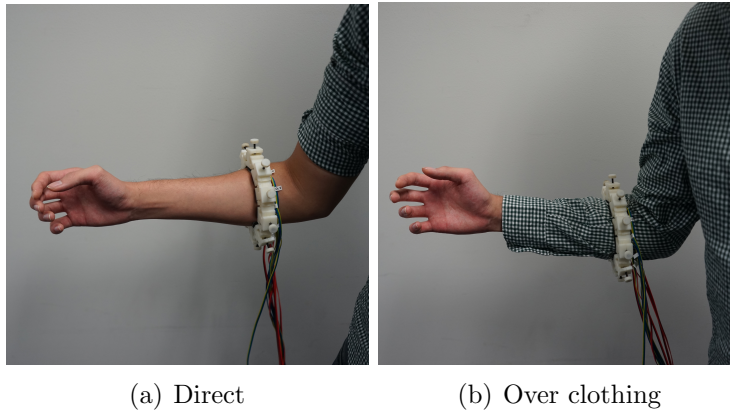


Fig. 19. Measurement conditions

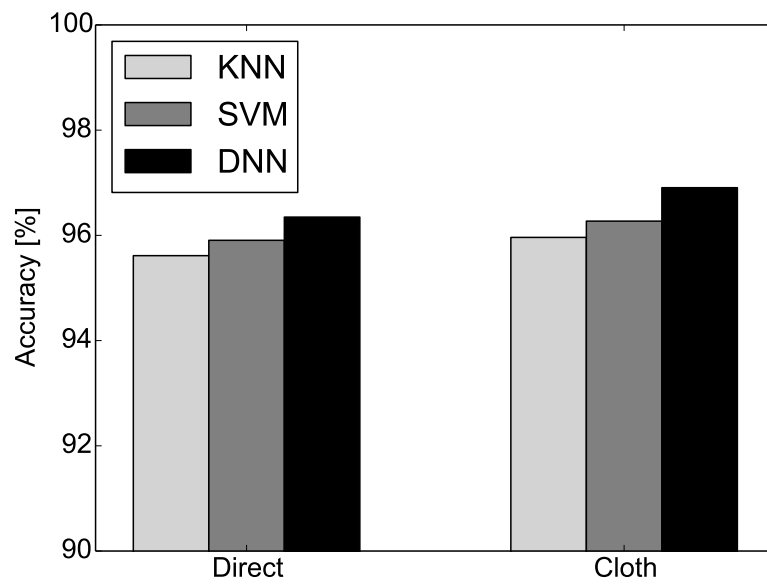


Fig. 20. Accuracy of each measurement condition

3.3 Discussion

The proposed method was able to accurately recognize seven different hand motions with various users. In particular, with all subjects, the accuracy of recognition of pronation and supination was also higher. In the forearm, the round pronator and supinator muscles are deep layer muscles. Pronation and supination of the forearm are caused by the activities of these muscles, and are important motions in the manipulation of objects in daily life.

For comparison, in a previous study using the sEMG [27], the accuracy of recognition of pronation and supination was under 90%, because sEMG is difficult to detect the activities of the deep layer muscles. This is an advantage of the proposed method when compared to other studies of the hand motion recognition based on the sEMG.

Our proposed method achieved better or similar performance compared to previous studies based on the FMG which recognized similar motions [35, 36]. Unlike FMG-based methods, our method does not need to provide the fixture of the sensor whose shape is closely matched to the forearm, because our distance sensor array is fitted to the user's forearm by the sponge. Moreover, the developed sensor array could measure the forearm deformation at the position close to the elbow where various muscles are located. Comparing to other studies that also used distance sensor arrays [47–49] which measured deformation of the wrist, the back of the hand, or the longitudinal direction on the forearm, our method could obtain more information and recognize more hand motions from the activities of the deep layer muscles. From the result, this method indicated a useful and alternative measurement and recognition method for hand motion recognition compared with other previous methods.

In addition, both hand motions and elbow postures change the shape of the forearm. However, we confirmed that using training data of various elbow postures, the proposed method can recognize hand motions with different elbow postures. From this result, it seems that the proposed method could be used without restricting motions of other body parts of the user.

Also, we experimentally showed that this method could accurately recognize hand motions both with direct measurement and measurement over clothing. This is a useful ability for the input interfaces for prosthetic hands or robotic ex-

oskeletons. For example, some users like to wear clothing when using a prosthetic hand or robotic exoskeleton.

Finally, the results showed no large differences between the three types of classifiers. The DNN classifier was somewhat more accurate in recognizing the neutral and recognizing hand motions with various measurement conditions. Since high accuracy was obtained independently by each classifier, we concluded that measurement of forearm deformation using a distance sensor array produces data containing information for classifying hand motions.

Chapter4

Estimation of Upper Limb Pose Based on Forearm Deformation

For the motion/activity detection, it is enough to recognize types of motions. On the other hand, to measure the motions in daily life or continuous control for the robots/machines, we need not to recognize but to estimate pose (e.g., joint angles). However, the studies based on the bio-signal to estimate the poses of the upper limb are few with comparing the studies based on vision or inertial and magnetic information. If it is possible to estimate the continuous poses of the upper limb, the applications of the method based on the bio-signal will be expanding. Therefore, we propose two types of pose estimation methods based on forearm deformation and test the performance as follows:

Hand Joint Angle

To confirm the motion estimation at the level of the joint angle is possible, we try to estimate three types of joint angles related to six types of the motions which are target motions in the hand motion-type recognition: wrist flexion and extension, hand closing and opening, and forearm pronation and supination. By using Support Vector Regression (SVR) [55], we estimate those three types of joint angles based on forearm deformation.

Upper Limb Pose

To deal with various upper limb motions in daily life, we propose an estimation method of upper limb pose based on forearm deformation. In this method, we estimate the forearm, hand, and fingers poses as upper limb pose. By using a DNN-based estimation model, upper limb poses are estimated. We evaluate the performance of the method with single-axis motion and daily life motions.

4.1 Hand Joint Angle

To confirm the possibility of the motion estimation at the joint angle level, we propose a hand joint angle estimation method based on forearm deformation.

4.1.1 Method Overview

As shown in Fig. 21, first, we measure forearm deformation using our developed distance sensor array and hand joint angles using motion capture. Second, we train estimation models using SVR that estimates three types of joint angles. The angle θ_w is the joint angle related to wrist flexion and extension, the angle θ_h is the joint angle related to hand closing and opening, and the angle θ_f is the joint angle related to the pronation and supination of the forearm.

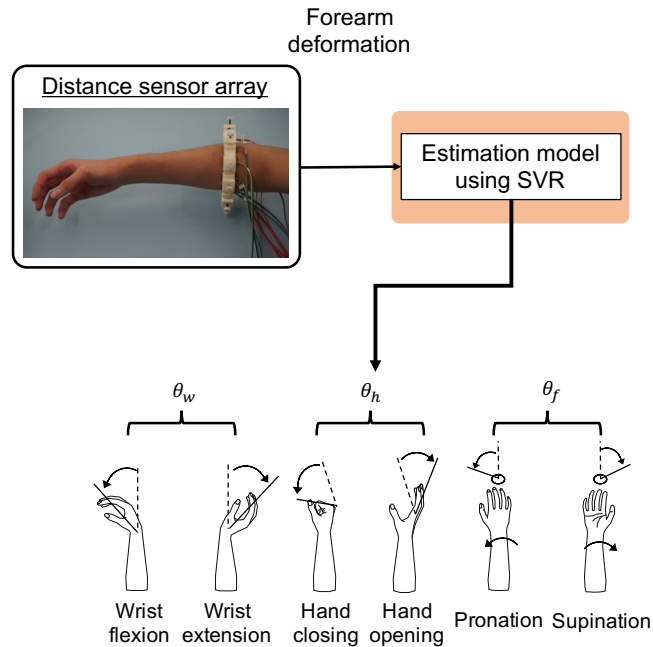


Fig. 21. Overview of the estimation of hand joint angle

4.1.2 Signal Measurement & Feature Extraction

Fig. 22 shows the measurement setup used with the proposed method. We adjust the size of the array so that each channel sinks down at least 0.5 mm deflection in the neutral pose. In this study, the raw data of the distance sensor array is sampled at 2000 Hz using an analog-to-digital converter (USB-6218, National Instruments). The distance sensor units, the A/D converter, and a stabilized power source are connected with cables. The A/D converter and the Leap Motion are connected to a PC using USB cables.

The hand joint angles are measured using a Leap Motion [56], which is a device that can detect the hand position with an accuracy of 0.01 mm at about 60 Hz. The joint angles are acquired from the Leap Motion API using the functions of *Hand.direction().yaw()*, *Hand.grabAngle()*, and *Hand.palmNormal().roll()*. The *Hand.direction().yaw()* return the angles related to wrist flexion and extension (θ_w). The *Hand.grabAngle()* return the angles related to hand closing and opening (θ_h). The *Hand.palmNormal().roll()* return the angles related to pronation and supination of the forearm (θ_f).

We use 10-dimensional *APR* as feature vector and θ_w , θ_h , and θ_f as the target values. The signal of the distance sensor array is arranged with the frame rate of 62.5 (*APR*), and the target values are arranged to match the frame rate of the *APR*.

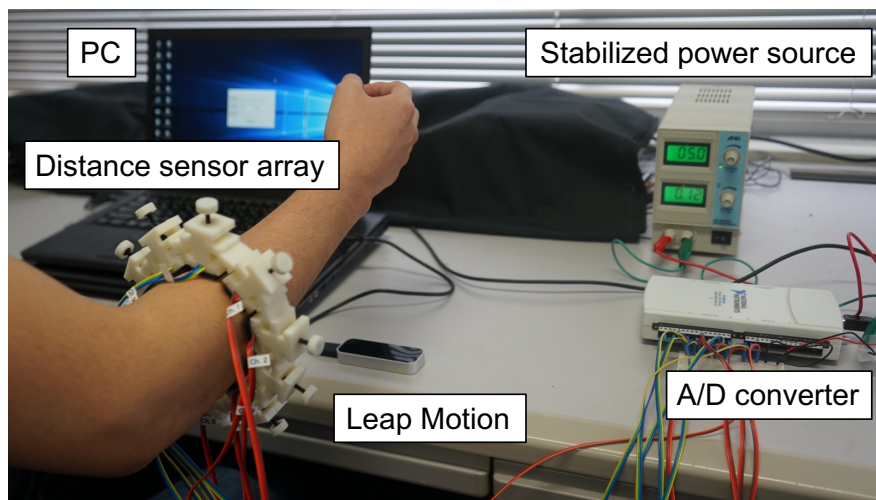


Fig. 22. The measurement setup for the estimation of the hand joint angle

4.1.3 Joint Angle Regression by SVR

In the proposed method, we use an SVR for joint angle regression. The input of the model is a 10-dimensional *APR*. The output of the model is a joint angle acquired from the Leap Motion. A radial basis function (RBF) kernel is used in our method. As shown in Fig. 23, three types of the joint angles are estimated by each model.

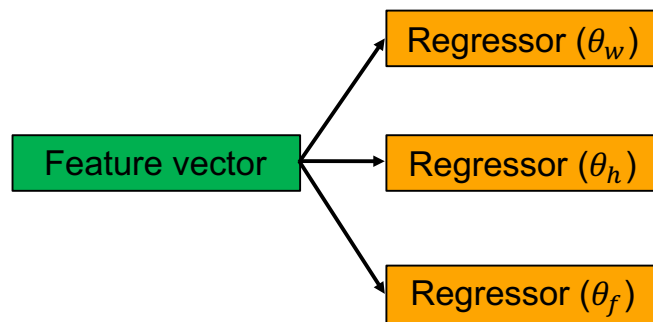


Fig. 23. Flow of the estimation

4.1.4 Experiments

We describe the experimental methods and results of the hand joint angle estimation experiments that we performed to test our proposed method. The experimental protocol was approved by the research ethics board of the Nara Institute of Science and Technology. Before participation in the experiments, informed consent was obtained from the subjects.

Conditions We performed experiments with five healthy subjects, A to E (the 20’s, male, right-handed).

The protocol of the experiments was the same as experiment 1 of chapter 3. In this experiment, each subject performed five trials. When performing the hand motion, the subject placed their hand so that the wrist joint was positioned above the Leap Motion. Using the Leap Motion, we collected the data.

For each subject, the five-trial data was then tested using five-fold cross-validation. We used four-fifth of the data for training, one-fifth of the data for testing. The number of frames for each trial was 3747. The length of the training data was $3747 \times 4 = 14988$ frames and the length of the testing data was 3747. In this experiment, we used $\gamma = 2$ and $C = 256$ for the hyperparameters of the SVR. These values were experimentally selected.

The accuracy of the proposed method was evaluated in terms of the root mean squared error (RMSE). The RMSE of each joint angle was calculated as follows:

$$\text{RMSE} = \sqrt{\frac{1}{M} \sum_{m=1}^M (\theta_{\text{Leap}}(m) - \theta_{\text{Estimated}}(m))^2}, \quad (8)$$

where M is the total number of frames for the testing data, θ_{Leap} is the joint angles acquired from the Leap Motion API, and $\theta_{\text{Estimated}}$ is the estimated joint angles using the proposed method in the m^{th} frame.

Results As an example of how closely the estimated joint angles and the measurements of the Leap Motion match, Fig. 24 shows the results of the hand joint angle estimation in one trial. Table 3 shows the RMSE of the estimated joint angles for each subject and the total for all subjects. This shows that the proposed method estimated the hand joint angle with the RMSE of 6.6 degrees for all joint angles. Specifically, the totals of RMSE for all subjects were 4.6 degrees for θ_w , 6.6 degrees for θ_h , and 5.3 degrees for θ_f .

The RMSE of θ_f related to the pronation and supination of the forearm was 5.3 degrees. This shows that the proposed method can estimate the hand joint angle from the activities of the deep layer muscles. Moreover, the maximum RMSEs for all subjects were 5.7 degrees for θ_w , 7.8 degrees for θ_h , and 5.9 degrees for θ_f . This shows that our method has the possibility to be applied to various users.

As shown in Fig. 24, no sudden erroneous estimation occurred between each hand joint angle. Moreover, there was no large phase lag between the estimated hand joint angles and the actual hand joint angles. In other words, the estimated angles and the measured angles were matched closely.

Table 3. RMSE for each subject on the hand joint angle estimation

Subjects	θ_w [deg]	θ_h [deg]	θ_f [deg]
A	4.0	4.9	5.3
B	5.7	6.7	5.1
C	4.6	7.6	5.2
D	4.6	7.8	4.8
E	4.0	5.7	5.9
Total	4.6	6.6	5.3

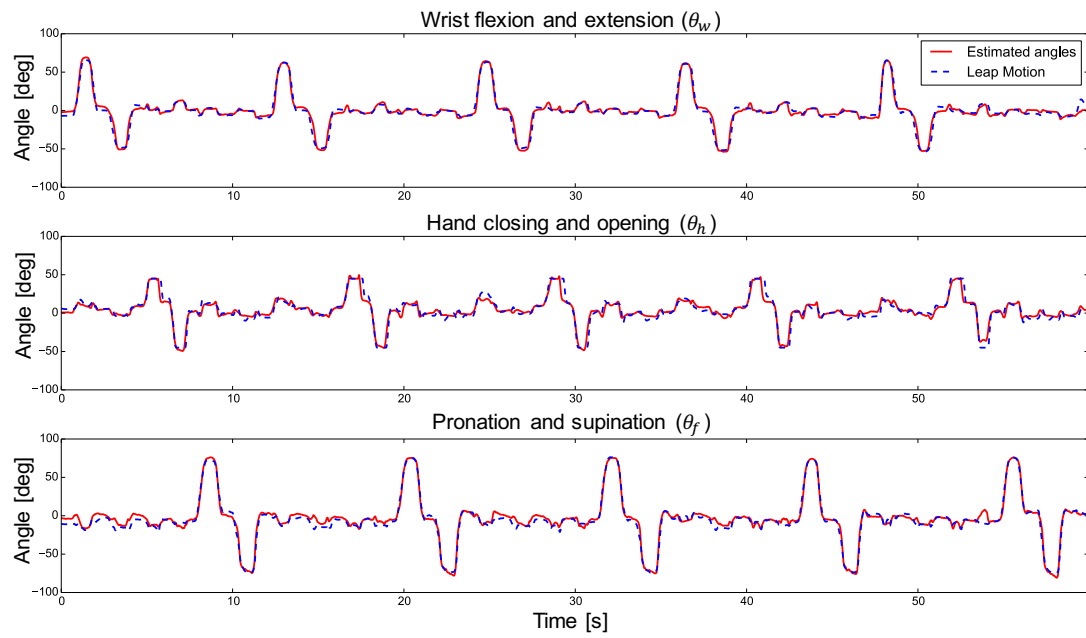


Fig. 24. An example of the results of the hand joint angle estimation

4.2 Upper Limb Pose

From the results of the experiments for the estimation of the hand joint angle, we confirmed that the estimation of the joint angle is possible by using forearm deformation. Moreover, from the experiments of the motion recognition, the shape of the forearm is changed with an elbow pose. In other words, the forearm deformation provides the motion information about not only the hand but also the elbow joint.

In this section, we expand the method to estimate the upper limb pose and evaluate the performance of the method on not only single-axis motions that move each axis independently but also daily life motions.

4.2.1 Method Overview

As shown in Fig. 25, first, we measure forearm deformation using our developed distance sensor array and upper limb pose using motion capture. Second, we train a DNN that estimates the upper limb pose. In this method, we estimate the poses of the forearm, hand, and five fingers.

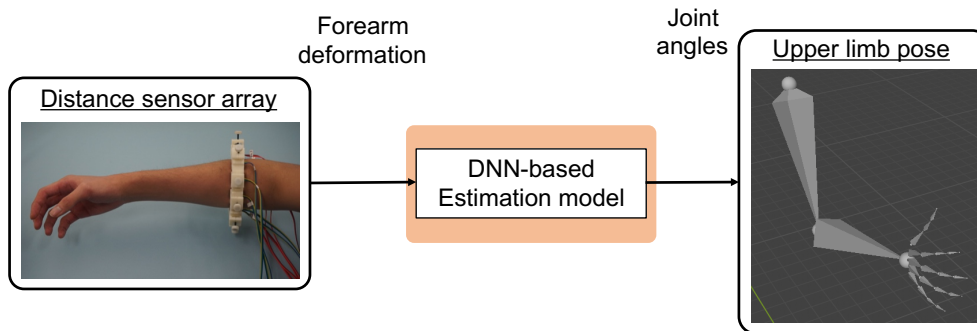


Fig. 25. Overview of the upper limb pose estimation

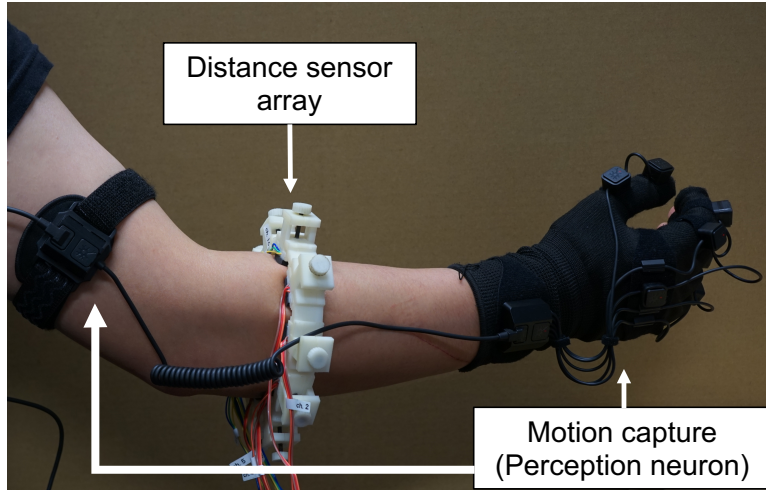


Fig. 26. Measurement setup for the upper limb pose estimation

4.2.2 Signal Measurement & Feature Extraction

As shown in Fig. 26, in this method, we measure forearm deformation using our developed distance sensor array and upper limb pose using a motion capture (Perception Neuron 2.0) [57]. We adjust the size of the array so that each channel sinks down at least 0.5 mm deflection in the elbow extension pose. The motion capture can measure poses of the forearm, hand, five fingers as a BVH format. As shown in Fig. 26, the sensors of the motion capture are set on the upper arm, forearm, hand, and five fingers. The distance sensor array and an A/D converter (USB-6218, National Instruments) are connected with cables. The A/D converter and the motion capture device are connected to the PC with USB cables. The signal of the distance sensor array is measured at 2000 Hz and the signal of the motion capture is measured at about 120 Hz.

The outputted values of the motion capture is 23 axes as follows:

Forearm

3 axes: Y-forearm, X-forearm, Z-forearm

Hand

3 axes: Y-hand, X-hand, Z-hand

Distal, middle, and proximal of the thumb

5 axes: Y-thumb1, Z-thumb1, Y-thumb2, Z-thumb2, Y-thumb3

Distal, middle, and proximal of four fingers

3 axes: Z-index1, Z-index2, Z-index3

3 axes: Z-middle1, Z-middle2, Z-middle3

3 axes: Z-ring1, Z-ring2, Z-ring3

3 axes: Z-pinky1, Z-pinky2, Z-pinky3.

The outputted values of the motion capture are calculated by the Euler angle of YXZ-rotation.

We use a 10-dimensional *APR* as a feature vector and the outputted 23 axes from the motion capture as the target values. For the upper limb pose estimation, the signal of the distance sensor array is arranged with the frame rate of 62.5 (*APR*), and the signal of the motion capture is arranged to match to the frame rate of the *APR*. Fig. 27 and Fig. 28 shows an example of the *APR* and acquired poses. The measured motions are as follows: elbow extension: EE, forearm pronation and supination: PR and SU, wrist flexion and extension: WF and WE, radial and ulnar flexion: RAF and UF, thumb flexion: TF, index flexion: IF, middle flexion: MF, ring flexion: RIF, and pinky flexion: PF.

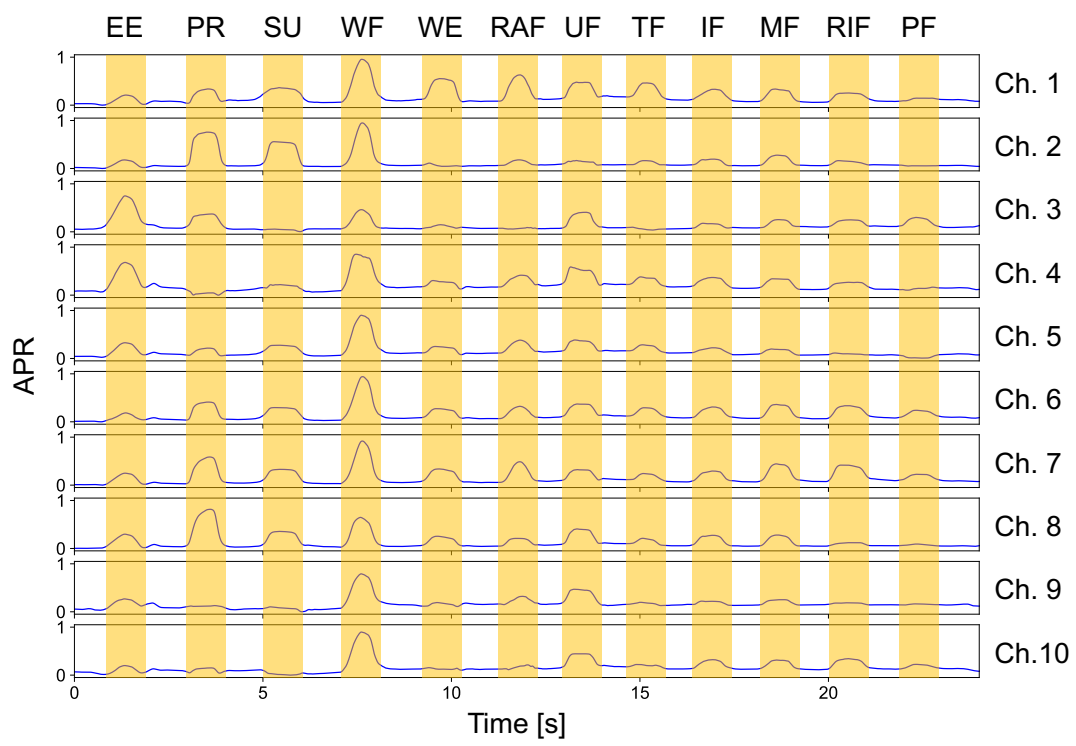


Fig. 27. APR of each channel with upper limb motions

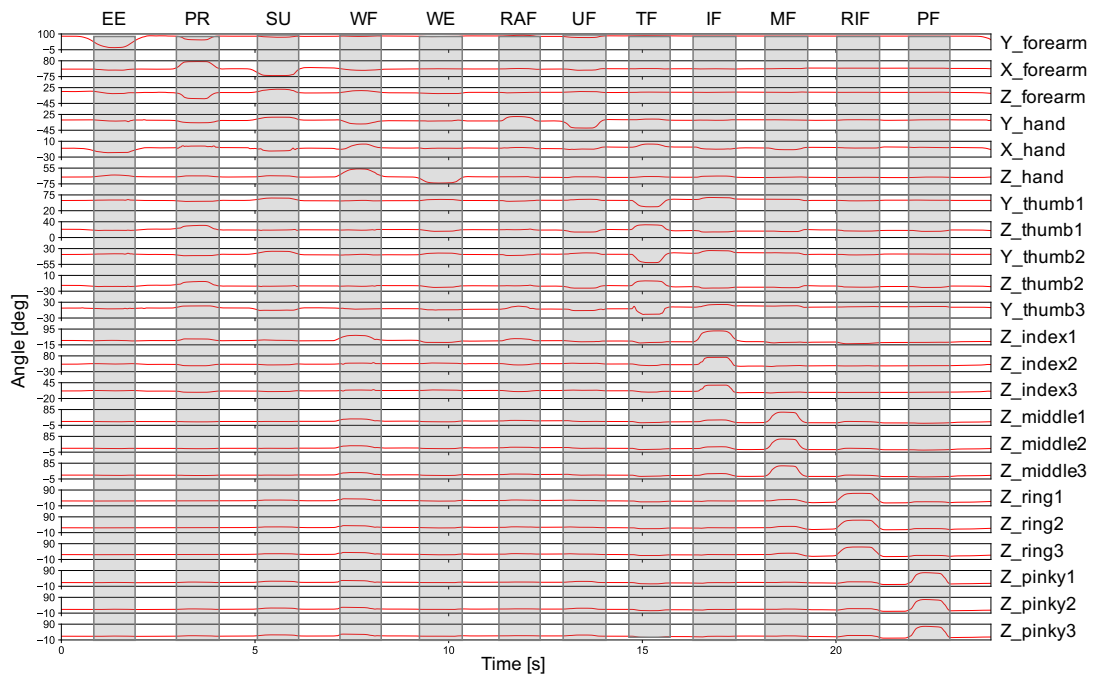


Fig. 28. An example of the acquired angles

4.2.3 Upper Limb Pose Estimation by DNN

In this method, we use a DNN to estimate the upper limb pose, as shown in Fig. 29. The DNN-based model consists of input and output layers and six hidden layers.

To consider a time series of the forearm deformation, we use data of about one second (60 frames) from the target frame to past as input. Thus, the number of the node of the input layer (N_{in}) is 600 (60 frames \times 10-dimensional APR). The number of the node of the output layer (N_{out}) is 23. The number of hidden layers is six. The numbers of nodes of the hidden layers (N_{hidden}) are 500, 400, 300, 200, 100, and 50. A ReLU is used as the activation function of each layer. A mean squared error is used as the loss function. The structure of the network is experimentally determined.

An Adam is used as an optimizer. The model is trained with a batch size of 32 and 50 epochs. The score of the training is checked with the loss of the training data. When the loss of the training data is not decreased during two epochs, the model training is stopped. The weights of the best score for the training data are used.

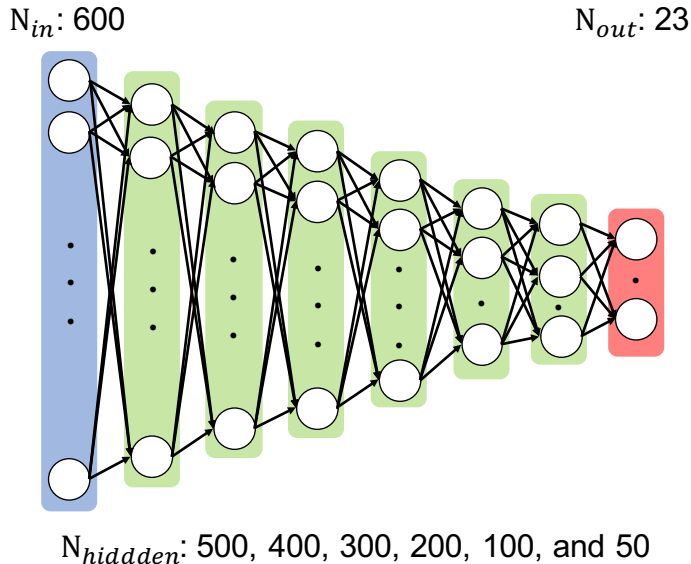


Fig. 29. Structure of the network for the upper limb pose estimation

4.2.4 Experiments

To evaluate the performance of the method, we performed estimation experiments of upper limb poses. We verified the performance with two types of experiments as follows:

Experiment 1: Single-axis motion

First, to confirm the possibility of the upper limb pose estimation based on only forearm deformation, we tested to estimate single-axis motions. In the experiment 1, subjects moved their upper limb with the following motions: elbow extension and flexion, forearm pronation and supination, radial and ulnar flexion, wrist flexion and extension, and flexion and extension of five fingers.

Experiment 2: Daily life motion

Second, to confirm the performance of the estimation in the daily life motion, we tested to estimate seven types of upper limb motions: opening a cap of a bottle, putting the cap, grasping the bottle, pouring to the cup, putting the bottle, grasping a cup, and bring the cup to the mouth. Those target motions include the combined motions of the forearm, hand, and fingers.

The experimental protocol was approved by the research ethics board of the Nara Institute of Science and Technology. Before participation in the experiments, informed consent was obtained from the subjects.

Experiment 1: Conditions We performed this experiment with six subjects (five 20's and one 40's, five males and one female, right-handed). The subject repeat neutral (elbow flexion pose) and the other 12 upper limb motions with guide motions of a robot arm, as shown in Fig. 30. Upper limb motions were performed in the order of elbow extension, forearm pronation and supination, wrist flexion and extension, radial and ulnar flexion, and flexion of five fingers. Each motion was performed to the maximum angle in the movable range, and then returned to the neutral position in about one second. Each trial was five sets of 12 motions during 120 seconds. Each subject performed four trials.

For each subject, the four trial data were tested by the four-fold cross-validation. The feature vectors were then scaled and shifted as $\min = 0$ and $\max = 1$. The number of frames for one trial was 7437. We used three trial data for training (22311) and the remaining one trial data for testing (7437). The performance of the method was evaluated with the RMSE and a percentage of RMSE in a moving range of the target motions.

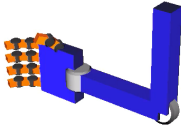

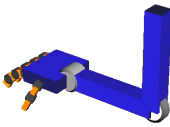
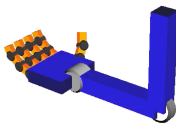
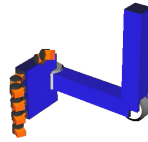
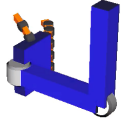
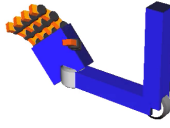
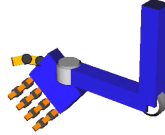
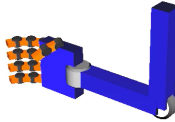
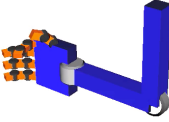
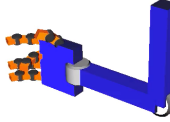
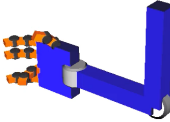
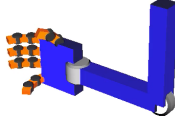
Neutral & Elbow flexion			
			
Elbow extension	Forearm pronation	Forearm supination	Wrist flexion
			
Wrist extension	Radial flexion	Ulnar flexion	Thumb flexion
			
Index flexion	Middle flexion	Ring flexion	Pinky flexion
			

Fig. 30. Guide motions of a robot arm

Experiment 1: Results Fig. 31 shows an example of the estimation results. The red line shows estimated angles and the broken blue line shows target angles acquired from the motion capture. In all of the axes, the estimated and target angles were matched closely.

Fig. 32 shows the RMSE of each joint angles for all subjects. The RMSE of all joint angles was 6 degrees or less. Fig. 33 shows the harmonic mean of the percentage of RMSE in the moving range for all subjects. In the experiment 1, the percentage of RMSE in the moving range was small for the forearm and hand. The percentage of RMSE in the moving range was high for the fingers compared with the forearm and hand. Though, the percentage of RMSE in the moving range was 8% or less for all axes.

Fig. 34 shows the estimation results with plotting by a BVH viewer. The left one is the estimated poses and the right one is the target poses. All of the poses were accurately estimated compared with the target poses.

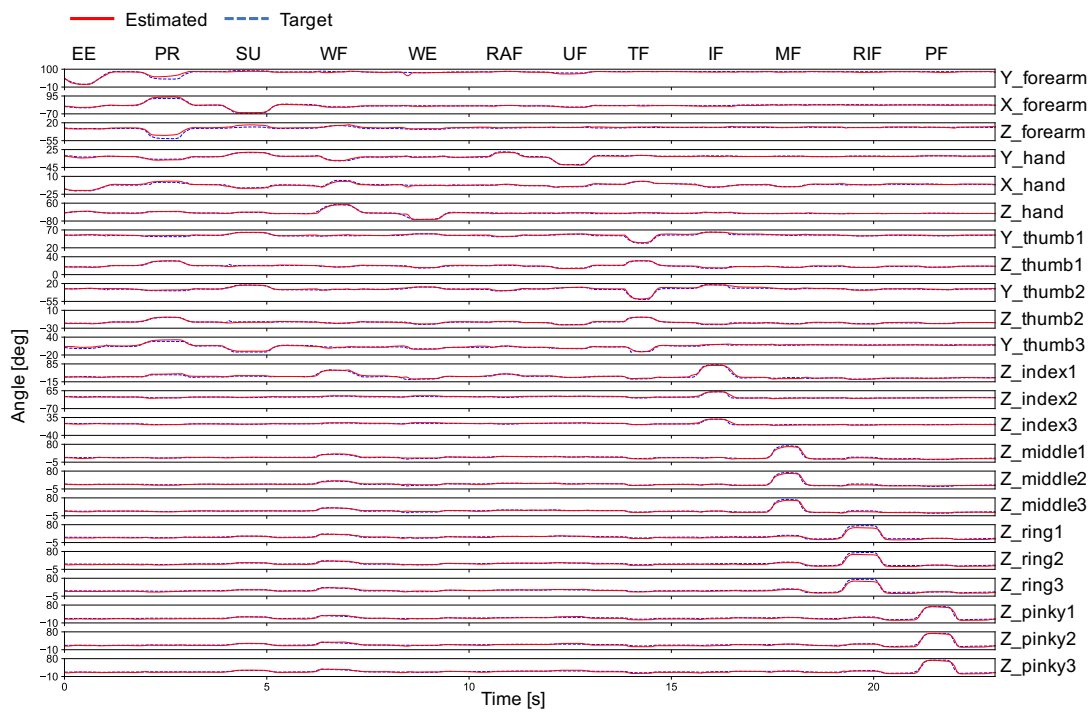


Fig. 31. An example of the estimated and target poses in the experiment 1

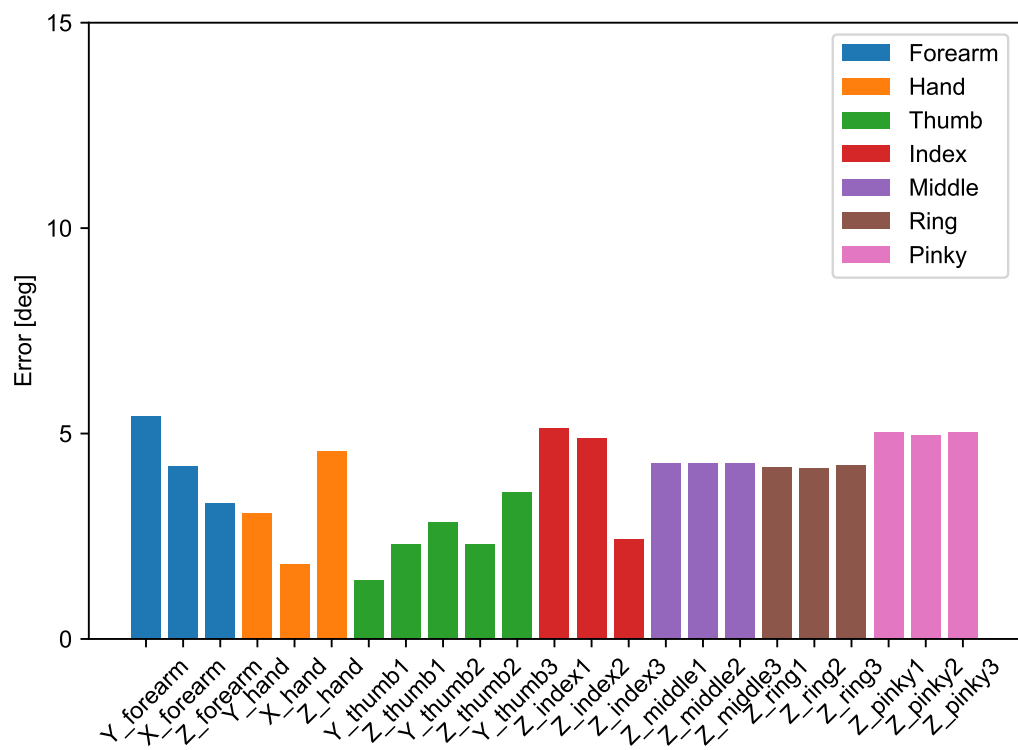


Fig. 32. RMSE of each axis in the experiment 1

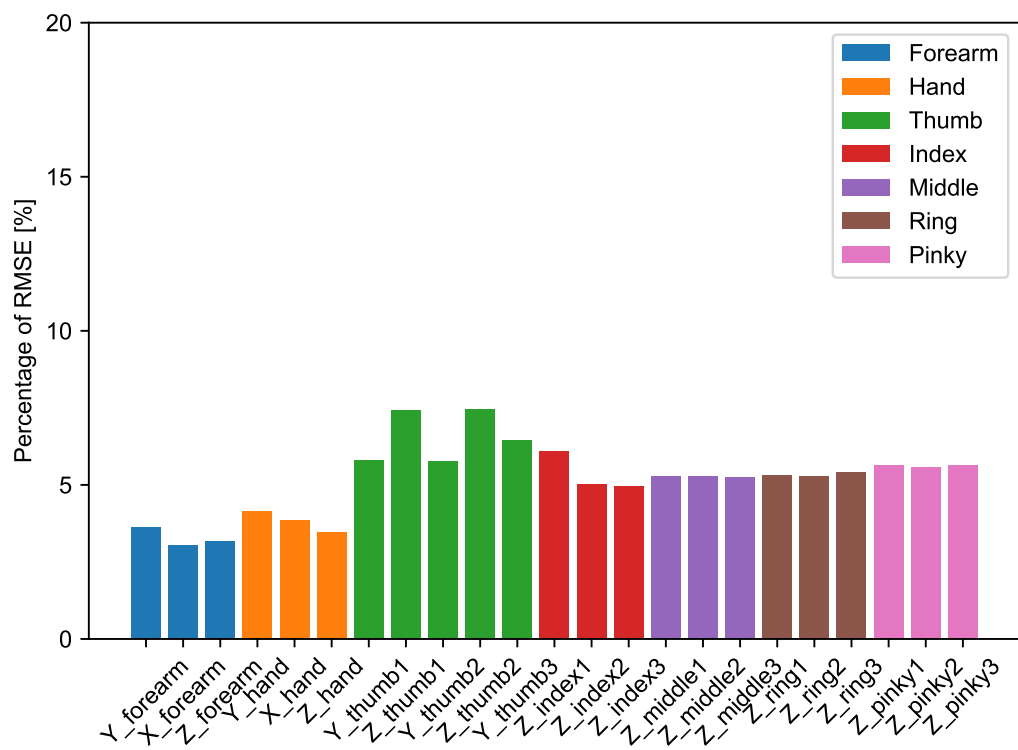


Fig. 33. RMSE in the moving range of each axis in the experiment 1

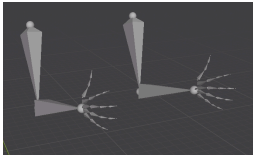
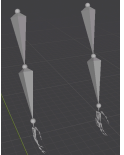
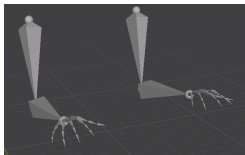
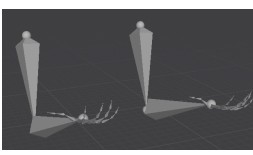
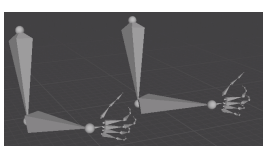
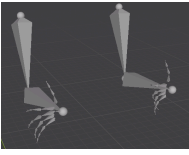
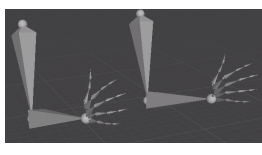
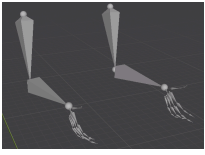
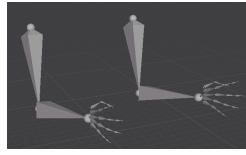
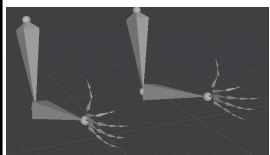
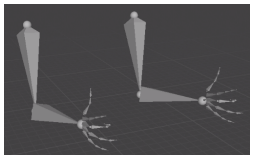
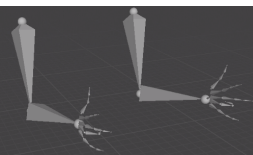
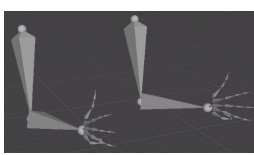
Neutral & Elbow flexion			
		Left: Estimated pose	Right: Target pose
Elbow extension	Forearm pronation	Forearm supination	Wrist flexion
			
Wrist extension	Radial flexion	Ulnar flexion	Thumb flexion
			
Index flexion	Middle flexion	Ring flexion	Pinky flexion
			

Fig. 34. An example of the estimated and target poses with BVH viewer in the experiment 1

Experiment 2: Conditions We performed this experiment with five subjects (four 20's and one 40's, four males and one female, right-handed). As shown in Fig. 35, subjects were asked to perform the following procedure of seven types of upper limb motions: opening a cap of a bottle, putting the cap, grasping the bottle, pouring to the cup, putting the bottle, grasping the cup, and bring the cup to the mouth. In this experiment, we did not decide the speed of the motions. So, the subjects performed the motions with their speed. Each subject performed the procedure ten trials.

The ten trial motions were tested with ten-fold cross-validation. We used nine trial data for training and the remaining one trial data for testing. The performance of the method in experiment 2 was also evaluated with the RMSE and a percentage of RMSE in a moving range of the target motions the same as the experiment 1.

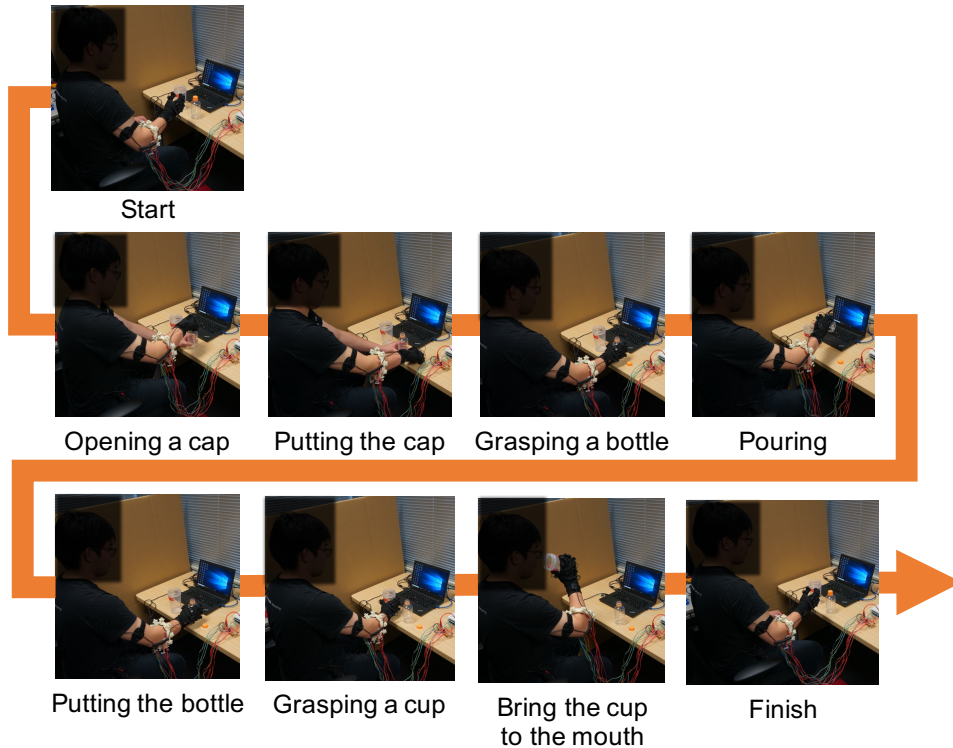


Fig. 35. Target motions in the experiment 2

Experiment 2: Results Fig. 36 shows an example of the estimation results. The estimated and target angles were matched.

Fig. 37 shows the RMSE of each joint angles for all subjects. The RMSE of all joint angles was 11 degrees or less. Fig. 38 shows the harmonic mean of the percentage of RMSE in the moving range for all subjects. In the experiment 2, the percentage of RMSE in the moving range was high for the hand, thumb, and index finger. Though, the percentage of RMSE in the moving range was 11% or less for all axes.

Fig. 39 shows the estimation results with plotting by the BVH viewer. The left one is the estimated poses and the right one is the target poses. All of the poses were accurately estimated compared with the target poses.

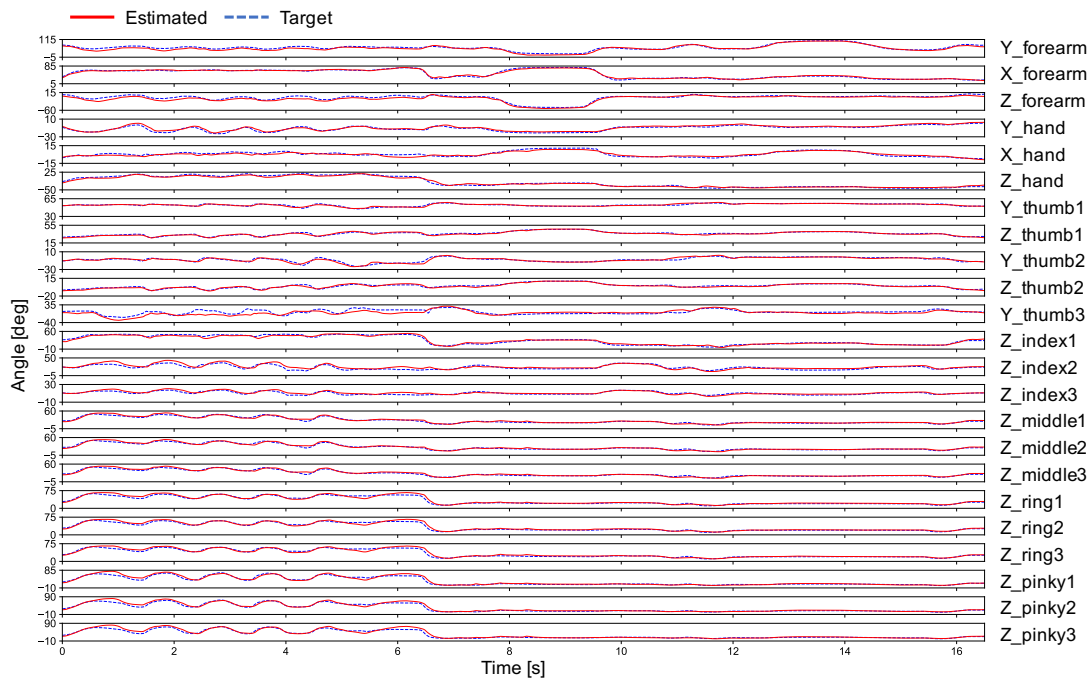


Fig. 36. An example of the estimated and target poses in the experiment 2

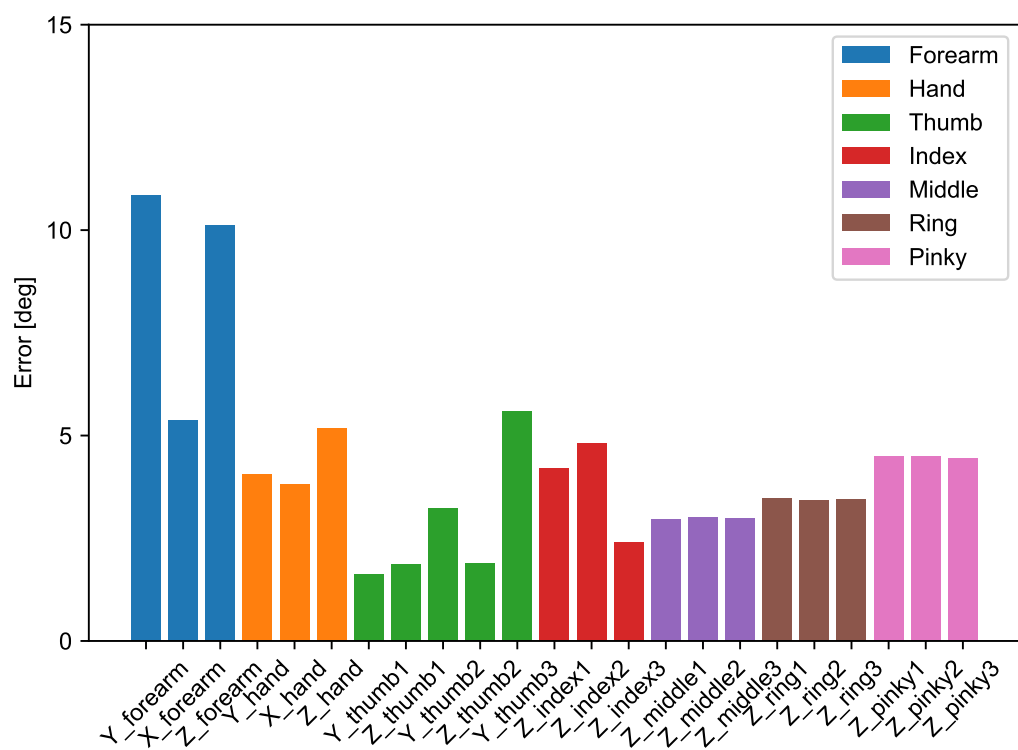


Fig. 37. RMSE of each axis in the experiment 2

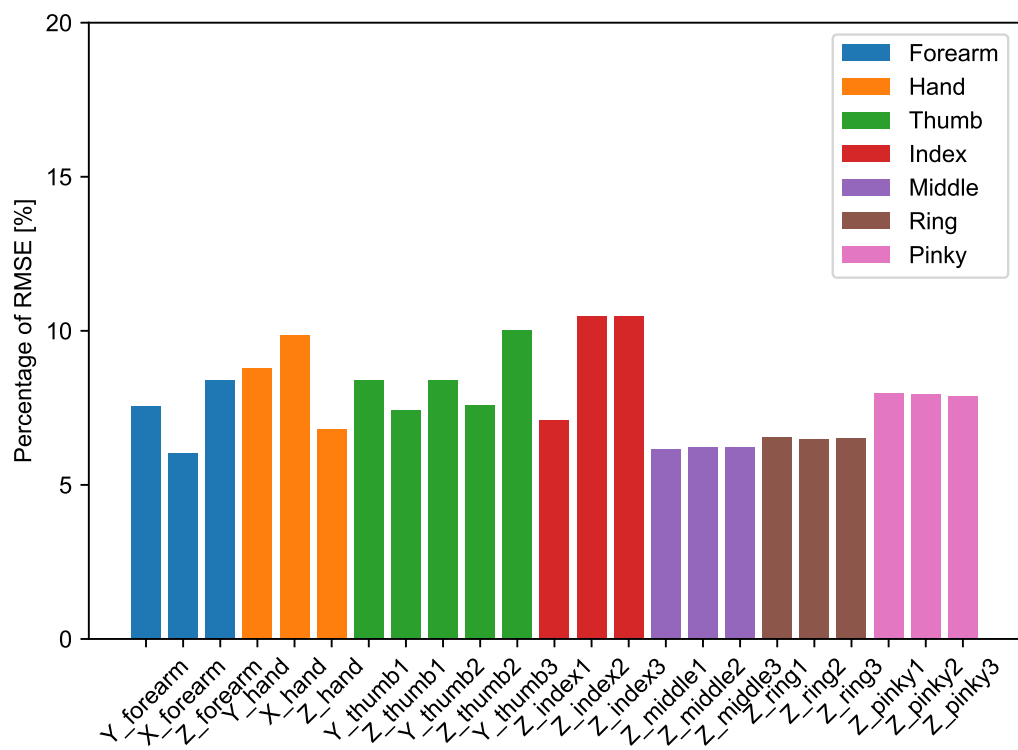


Fig. 38. RMSE in the moving range of each axis in the experiment 2

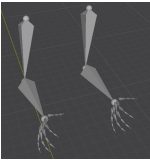
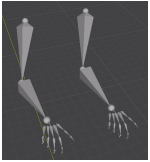
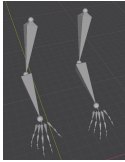
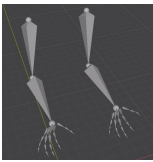
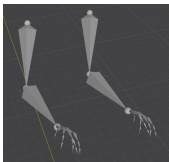
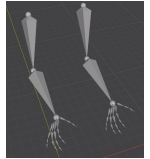
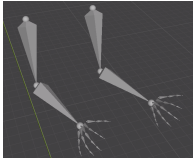
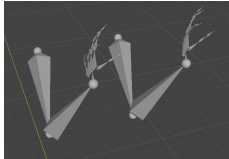
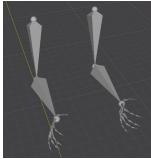
Start			
		Left: Estimated pose Right: Target pose	
Opening a cap	Putting the cap	Grasping a bottle	Pouring
			
Putting the bottle	Grasping a cup	Bring the cup to the mouth	Finish
			

Fig. 39. An example of the estimated and target poses with BVH viewer in the experiment 2

4.3 Discussion

From the results of the experiments, the upper limb pose estimation using the forearm deformation achieves better performance in not only single-axis motions but also daily life motions.

In experiments of the hand joint angle and upper limb pose estimation, the forearm deformation still shows a good performance to estimate motions related to the activities of the deep layer muscles. Moreover, to focus on a characteristic of the forearm deformation which the shape of the forearm is changed with elbow joint angles, the method realizes to estimate motions with elbow joint angles.

In the related research, Ngeo *et al.* [58] estimated the poses of the five fingers based on the sEMG. They set the eight-channel of the sEMG-sensors from the position close to the elbow to the position close to the wrist on the forearm. By using the measured signal, they realized the finger pose estimation.

On the other hand, our proposed method was able to estimate not only the fingers but also the forearm and hand motions. In particular, our method was able to estimate the pose of the upper limb using only the wearable device which is attached to the forearm position close to the elbow. Quivira *et al.* [59] estimated finger position and joint angles based on the sEMG on the position closed to the elbow. In their method, the RMSE of the finger joint angles is around 10 degrees. Our method achieved similar results in the method. Moreover, from our best knowledge, the study of the pose estimation at the multiple joint angles including the forearm, hand, and fingers based on bio-signal is nothing. Thus, our method showed a possibility to expand the application of the methods based on the bio-signals.

In addition, since the high performance with the method, we confirmed that measurement of forearm deformation using the distance sensor array also produces data containing information for estimation of upper limb pose.

Chapter 5

Forearm Pose Estimation Based on Upper Arm Deformation

The upper arm deformation also has rich information related to upper limb motions. To estimate the forearm poses with measurement of the upper arm deformation, we can provide the variation of the sensor attached position for various applications.

5.1 Method

We propose a method to estimate the pose of the forearm (flexion/extension, pronation/supination) based on the upper arm deformation. As shown in Fig. 40, first, we measure the upper arm deformation using the developed distance sensor array. Second, we train a DNN that estimates the elbow joint angle (θ_e) and the forearm pronation and supination angle (θ_f).

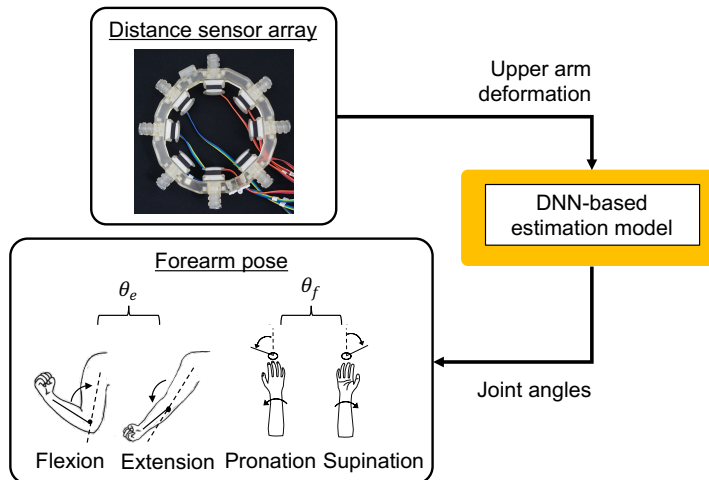


Fig. 40. Overview of the forearm pose estimation

5.1.1 Signal Measurement & Feature Extraction

We measure upper arm deformation using our developed distance sensor array. We adjust the size of the array so that each channel sinks down at least 0.5 mm deflection in the elbow extension pose and the neutral pose of the forearm. We also measure the forearm poses using a motion capture (OptiTrack) only for training, as shown in Fig. 41. Pairs of markers of the motion capture are attached on the shoulder, the elbow, and the wrist to estimate the joint positions.

The signals of the distance sensor array are read via an A/D converter (USB-6218, National Instruments). Due to the quality of the signals, a stable power source supplies the energy to the array. The A/D converter and a PC are connected with a USB cable. A motion capture system and the PC are connected with a LAN cable. The upper arm deformation is measured at 1200 Hz. Data on the motion capture is measured at 120 Hz.

We use a 8-dimensional *APR* as the feature vector and θ_e and θ_f as the target values of the estimation. In this method, the *APR* is obtained by averaging ten samples, which are re-sampled to synchronize the frame rate of the motion capture. The target values are calculated by the positions of the makers of the motion capture. Fig. 42 shows an example of the feature vectors and the forearm poses.

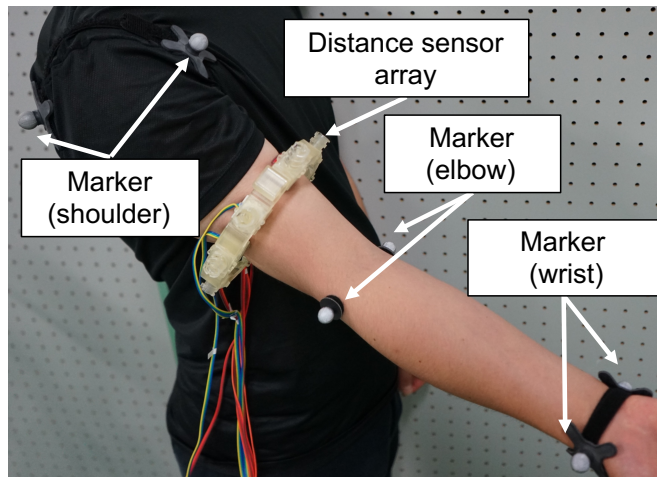


Fig. 41. Measurement setup for the forearm pose estimation

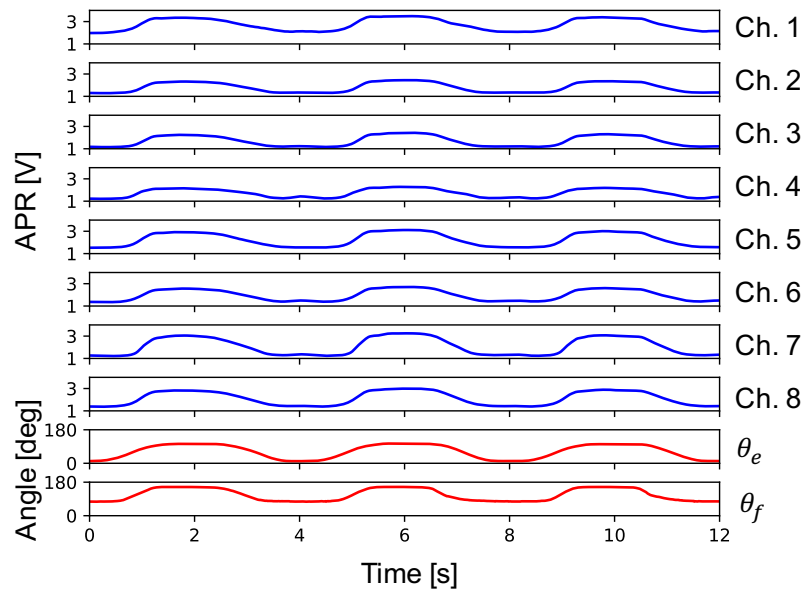


Fig. 42. An example of the feature vector and the forearm poses

5.1.2 Forearm Pose Estimation by DNN

Fig. 43 shows the architecture of the proposed model. A fully-connected multiple layer neural network model is used. The proposed model consists of input and output layers and four hidden layers. To consider a time series of the upper arm deformation, we use 25 frames data (12 frames before and after the target frames) as the input data. The number of the input nodes (N_{in}) is 200 (25 frames \times 8-dimensional APR). The number of the output nodes (N_{out}) is two (joint angles θ_e and θ_f). The numbers of the nodes of each hidden layer (N_{hidden}) are 100, 50, 25, and 12. A ReLU is used for the activation function for each layer. The structure of the network is experimentally determined.

An Adam is used as the optimizer, and the mean squared error is used as the loss function. The model is trained with a batch size of 128 and 150 epochs. The score of the training is checked with the loss of the training data. The weights of the best score for the training data are used.

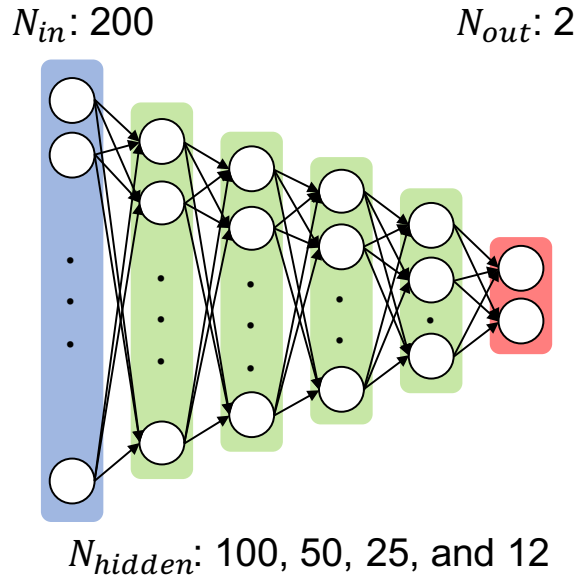


Fig. 43. Architecture of the model for the forearm pose estimation

5.2 Experiments

To confirm the performance of the proposed method, we performed a forearm pose estimation experiment. The experimental protocol was approved by the research ethics board of the Nara Institute of Science and Technology. Before participation in the experiments, informed consent was obtained from the subjects.

5.2.1 Conditions

We performed the experiment with five healthy subjects, A to E (the 20's, male, right-handed). The subjects wore the distance sensor array and motion capture marker and performed different motion: the elbow flexion and extension, and the pronation and supination of the forearm simultaneously. In this experiment, we asked the subjects to move their forearm with fixing the upper arm pose.

For each subject, 12 types of motions were measured in each of the following two conditions:

Condition 1

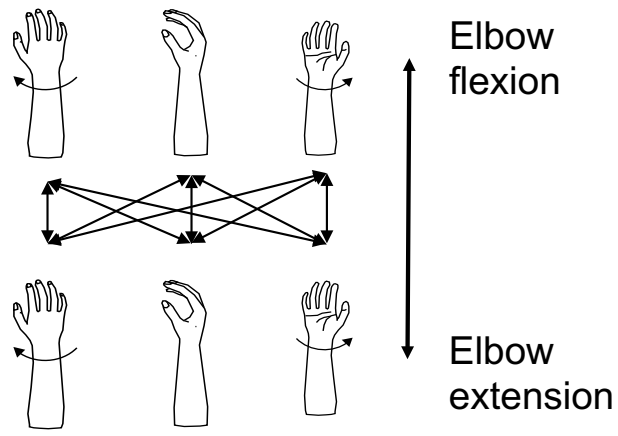
Subjects move between one of the three poses (pronation, neutral, and supination) in the flexing elbow and another pose in the extending elbow, as shown in Fig. 44(a). In one trial, the elbow flexion and extension were performed three times. Every subject performed nine types of movements.

Condition 2

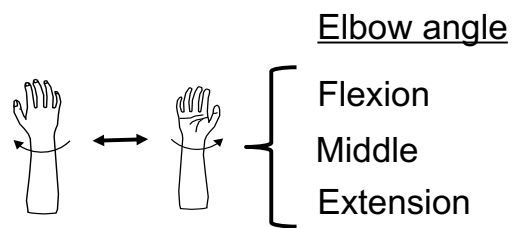
Subjects move their forearm from pronation to supination with a fixed elbow joint angle (flexion, middle, and extension), as shown in Fig. 44(b). In one trial, the forearm pronation and supination were performed three times. Three types of movements were performed by the subjects.

One trial was taken in 12 seconds. Subjects performed each motion five times. The total number of trials of all the patterns was $12 \times 5 = 60$.

For the evaluation, we tested 60 trial data with five-fold cross-validation. The feature vectors were then scaled and shifted as mean = 0 and variance = 1. Every four trial data of each pattern were used for training and the remaining one trial data of each pattern were used for testing. The number of one trial data was 1416. Thus, the number of the training data was 67968 and the number of the testing



(a) Condition 1



(b) Condition 2

Fig. 44. Measured motion conditions

data was 16992. The pose estimation model was trained with each subject. The performance of the proposed method was evaluated with the RMSE.

5.2.2 Results

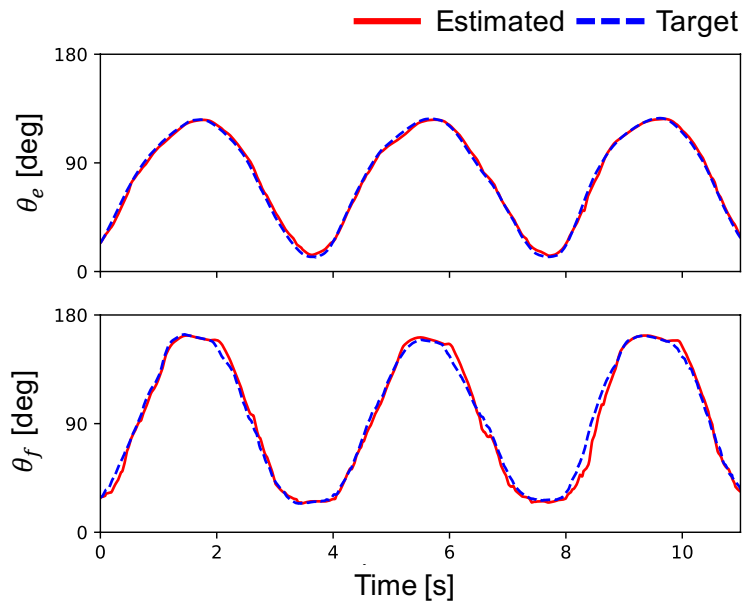
Fig. 45 shows the estimated results when the subject moved the forearm between supination/pronation and pronation/supination during the elbow flexion and extension in the condition 1. The red line shows the estimated joint angles and the broken blue line shows the target joint angles. In the condition 1, the estimated joint angles were matched to the target joint angles in both joints.

Fig. 46 shows the estimated results when the subject pronated and supinated the forearm when keeping the elbow joint angle in the condition 2. In the condition 2, the estimated joint angles were also matched to the target joint angles well in both joints.

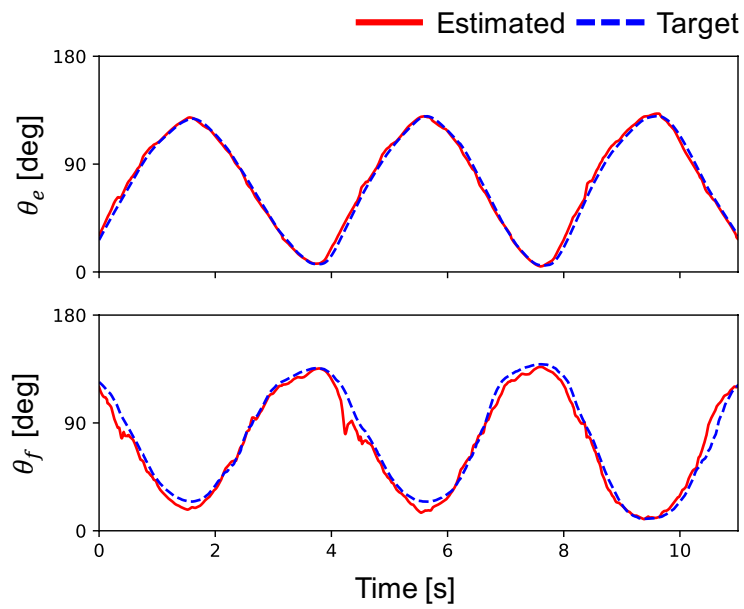
In both conditions, the method was able to estimate the two joint angles of the forearm pose. There was no large difference between the estimated pose and the target pose and no large phase difference. Table 4 shows the RMSE of each subject and the total for all subjects. The totals of RMSE for all subjects were 2.9 degrees for the θ_e , and 7.6 degrees for the θ_f . The maximum RMSEs of the joint angles were 3.9 degrees for the θ_e , and 10.1 degrees for the θ_f .

Table 4. RMSE for each subject on the forearm pose estimation

	θ_e [deg]	θ_f [deg]
A	2.4	6.4
B	2.5	7.8
C	2.5	6.8
D	3.2	6.3
E	3.9	10.1
Total	2.9	7.6

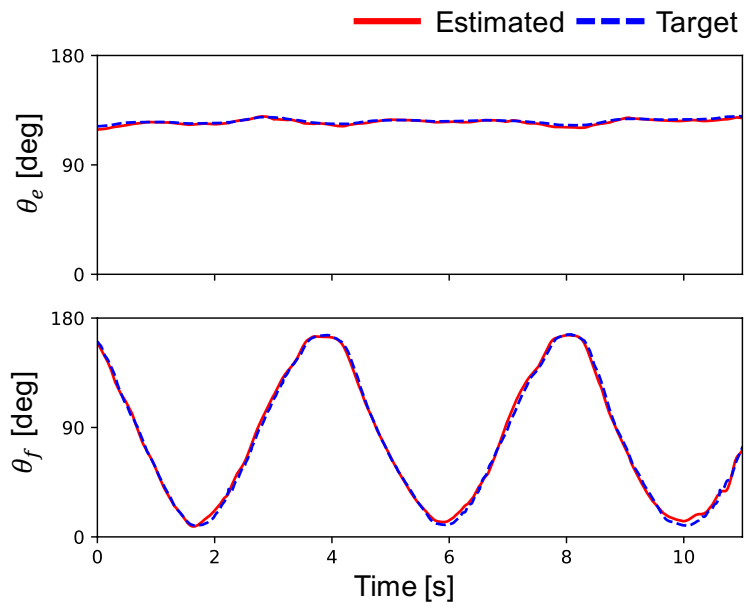


(a) Supination to pronation

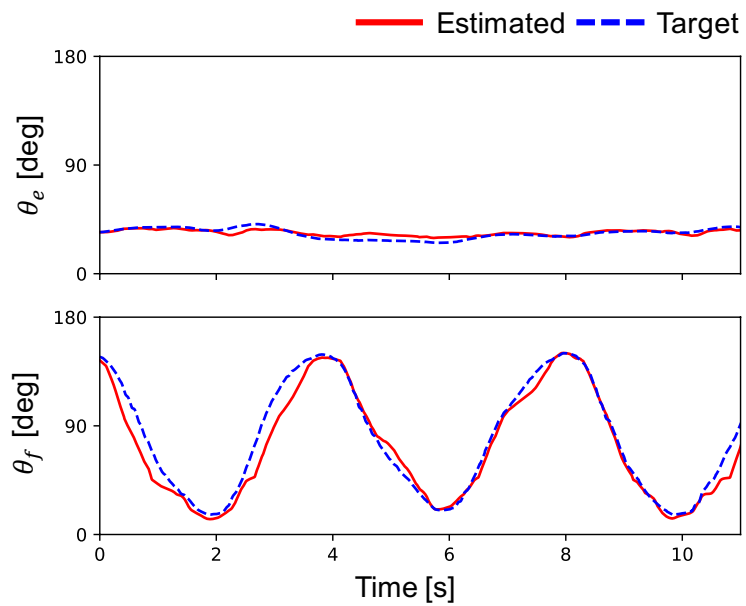


(b) Pronation to supination

Fig. 45. Estimation results on the condition 1



(a) Flexion



(b) Extension

Fig. 46. Estimation results on the condition 2

5.3 Discussion

The RMSE of the elbow joint angle (θ_e) was lower than that of the forearm pronation and supination angle (θ_f). This is because the muscles in the upper arm such as the biceps brachii and the triceps brachii muscles mainly contribute to the elbow flexion and extension. These muscles contribute to the forearm pronation and supination on a certain level, though several muscles in the forearm mainly work for these motions. It may be the reason that the RMSE of the θ_f is also not large.

In the condition 2, when comparing the estimation results of the θ_f between the flexion and extension of the elbow pose, the results of the flexion were better than those of the extension, as shown in Fig. 46. It is because the work of the biceps brachii muscle for supination becomes more dominant when the elbow joint was flexed. Since there were no large differences between the estimated and the target θ_f when the elbow joint was extended, our proposed method was able to estimate the θ_f . These results showed that our proposed method was able to estimate the forearm pose only from the upper arm deformation.

The method based on the sEMG [60] estimated the same joint angles of θ_e and θ_f which are targeted in our method. The RMSE of the elbow joint angle (θ_e) is around 10 degrees, and the forearm pronation and supination angle (θ_f) is around 20 degrees. They tested the performance with different motions. Although the accuracy is affected by the type of motion, it was confirmed that the proposed method has a similar or better performance with the existing method based on the sEMG.

Since high performance with the method, we confirmed that measurement of upper arm deformation using the distance sensor array produces data containing information for estimation of forearm pose. Upper arm deformation showed a possibility to provide the variation of the sensor attached position for the various application.

Chapter6

Analysis and Discussion

In this chapter, we describe an analysis and a discussion about the skin deformation and applications of our proposed methods. We compare the difference between the skin deformation and the sEMG. In addition, we discuss potential applications and demands that need to be satisfied.

6.1 Comparison Between the Skin Deformation and the sEMG

Table 5 and 6 show the functions of the muscles of the forearm and the upper arm [61]. The muscles mentioned above related one or two motions. For example, in the forearm case, the extensor carpi radialis contributes both the wrist extension and the radial flexion. Fig. 47 shows the forearm deformation measured with the developed distance sensor array in both the wrist extension and the radial flexion. The gray and blue lines indicate the shape of the forearm in the neutral and the shape after the motion, respectively. The shape of the neutral was decided to be similar to the actual shape. When attaching the array on the forearm, Ch. 1 was set on the top of extensor carpi radialis. Thus, in both poses, Ch. 1 captured the activities of the extensor carpi radialis through the deformation.

Moreover, when the motion is even a single joint movement, multiple muscles contribute to the motion. In the multiple joints movement case, Sato *et al.* [62] reported that the forearm pronation force is different between the pose of wrist flexion and wrist extension. The combination of the many muscles causes varieties of motions.

Table 7 shows the differences between the sEGM and skin deformation. The sEMG and the skin deformation have advantages and limitations independently. The differences are three: measurement conditions, target tissues, and acquired signals.

The first one is the measurement conditions. The sEMG needs to attach a

Table 5. Functions of the forearm muscles

Muscle	Functions
Flexor carpi radialis	Wrist flexion and radial flexion
Flexor pollicis longus	Thumb flexion
Flexor carpi ulnaris	Wrist flexion and ulnar flexion
Flexor digitorum superficialis	2-5th finger PIP flexion and wrist flexion
Flexor digitorum profundus	2-5th finger DIP flexion and wrist flexion
Extensor carpi radialis	Wrist extension and radial flexion
Extensor digitorum communis	2-5th finger extension and wrist extension
Extensor carpi ulnaris	Wrist extension and ulnar flexion
Brachioradialis	Elbow flexion and moving the forearm to neutral
Palmaris longus	Wrist flexion
Round pronator	Forearm pronation
Supinator	Forearm supination

Table 6. Functions of the upper arm muscles

Muscle	Functions
Biceps brachii	Elbow flexion and forearm supination
Triceps brachii	Elbow extension
Brachialis	Elbow flexion

sensor on the skin directly. An advantage of the skin deformation is that it can measure the signal both direct on the skin or over the clothing.

The second one is the target tissues. The target tissues of the sEMG are the muscles, and those of the skin deformation are the muscles, bones, and tendons.

The third one is the acquired signals. By using the sEMG, we can acquire the activities of the muscles which are located just below a sensor. By using the skin deformation, we can get the activities of the muscles, bones, and tendons as deformation of the whole circumference. When we need to measure the activity of the pinpointed muscle and when the target muscle is one of the surface layer muscles, the measurement of the sEMG is a useful way. This is an advantage of the sEMG. The measurement of the sEMG of surface layer muscles is used for a kind of ground truth or an evaluation index of the motion analysis [63]. On

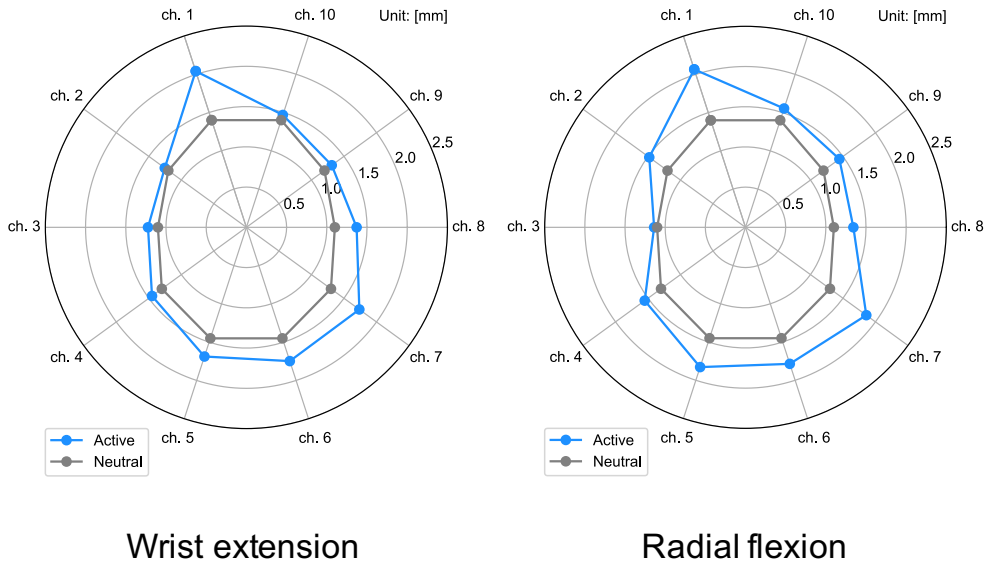


Fig. 47. Forearm deformation measured with the developed distance sensor array in the poses of wrist extension and radial flexion

the other hand, the detection of the activity of the pinpointed muscle using the skin deformation is more difficult than the sEMG, since the skin deformation is a complex signal. The skin deformation is caused by the activities of the muscles, bones, and tendons. When we need to comprehend these activities as the whole deformation, the measurement of the skin deformation is a useful way.

In short, the skin deformation has the advantage in measurement conditions and acquired signals compare with the sEMG. In the forearm case, the round pronator and supinator muscles are mainly related to the forearm pronation and supination. On the other hand, other muscles are also related to the motions. The sEMG-based methods should be use the activities of the other muscles to estimate the motions.

The skin deformation can also get the displacement of the bones. Fig. 48 shows that forearm deformation measured with the distance sensor array and cross-section measured with an MRI. In the pronation and supination motions, the radius bone is displaced by the muscle activity. By the displacement of the bone, the shape of the cross-section is changed. This difference may be the reason

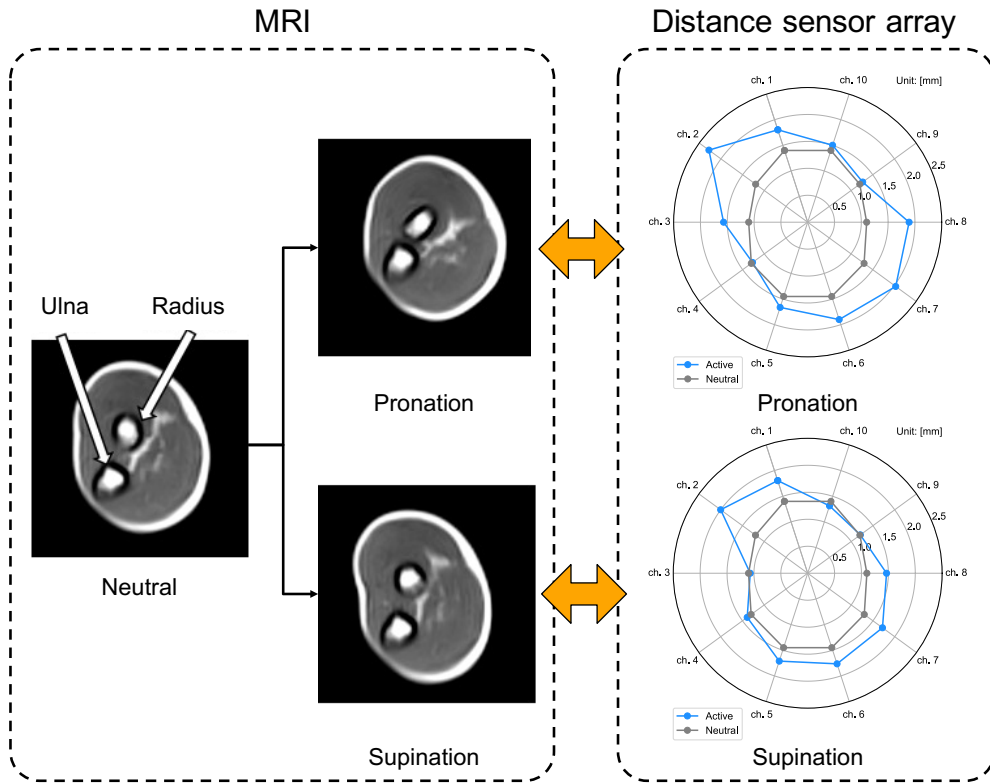


Fig. 48. Forearm deformation measured with the distance sensor array and cross-section measured with an MRI in the pose of pronation and supination

why our proposed method could robustly recognize the motions from the activities of deep layer muscles.

Table 7. Differences between the sEGM and skin deformation

	sEMG	Skin deformation
Measurement condition	Direct on the skin	Direct on the skin, Over clothing
Target tissues	Muscles	Muscles, bones, and tendons
Acquired signals	the activity of the muscle just below the sensor	Deformation of whole circumference

6.2 Potential Applications

Hand motion recognition

The hand motion recognition method could be applied to the input interface of the command control. For example, the current prosthesis hands are controlled by the command corresponding to the hand motion which is predicted/recognized by some machine learning-based methods or rule-based methods. Our proposed method can be applied to the interface, since the method could robustly recognize seven different types of hand motions including the motions from the activities of the deep layer muscles. Moreover, the skin deformation could be measured with over clothing by using developed distance sensor array and the performance of the hand motion recognition is kept even compared with measurement directly.

To apply the method to the input interface of the prosthesis hand, we need to consider the following two additional things. The first one is an attachment method of the distance sensor array. In the case of the prosthesis hand, users wear the sensor array on the amputation stump of the forearm. When grasping heavy objects, the reaction is taken on the amputation stump. In this case, output signals of the sensor array are changed with not only motions but also the reaction. Therefore, the development of an attachment method of the sensor array which is insulated from the influence of the reaction is needed. The second one is a variety of the amputation stump of the forearm. For many reasons, the amputation stump of the users are different. The amount of the muscles and the length of the forearm is also different. Moreover, congenital users do not have a sense of motion. For these reasons, it is necessary to check which imaginary actions of the user the proposed method can recognize.

Upper limb pose estimation

The upper limb pose estimation method could be applied to not only input interface but also motion measurement in various fields. Our proposed method could estimate upper limb poses of not only single motion but also daily life motions using only a wearable device that is attached to the position close to the elbow. Therefore, by using the method, we may expand

a variation of the applied measurement condition and environment.

To apply the method in various fields, we need to develop a measurement system that can quickly get the target motions for the learning. In the experiments of the estimation of the upper limb pose, we used the motion capture based on the IMU and magnetic sensors. For daily use, it is difficult to use motion capture. Therefore, by using the existing method such as Simon's method [13], we may get the 3D poses using a camera only.

Forearm pose estimation

The forearm pose estimation method has the potential to apply to the control interface of the upper limb prosthesis hand and motion measurement. In the case of the forearm prosthesis hand, the sensor can be placed on the forearm. However, in the case of the upper arm prosthesis, the sensor cannot be placed. Since it was shown that the poses of the forearm could be estimated from the upper arm deformation, the sensor placement position can be selected according to the application.

For the upper limb prosthesis, we need to consider the additional work which is the same as the forearm prosthesis. Moreover, we also consider the pose of the upper arm. The shape of the upper arm is changed with the pose of not only the forearm but also the upper arm.

Bio-mechanical analysis

In this dissertation, we focused on motion estimation and clarified the performance of the skin deformation. The skin deformation has the potential to estimate upper limb motions. On the other hand, the skin deformation is caused by the activities of the body tissues such as deformation of the cross-section of the muscles, displacement of the bones, and expansion and contraction of the tendons. There is a possibility that the activities of the body tissues can be obtained from the skin deformation. If it is possible to estimate or calculate the activities, we can get more rich information in a non-invasive manner.

In the previous study, Sagawa *et al.* [63] estimated the muscle activity and joint angles of the lower limb based on the 3D shape of the lower limb

measured with a projector-camera system. It showed that the activity of the muscle could be estimated by the skin deformation.

Difficulties for the bio-mechanical analysis are that the parameters of the skin deformation are too high and the ground truth of the activities of body tissues is hard to get. Especially, measurement of the activities of the deep layer muscles is difficult in a non-invasive manner.

To analyze or estimate the activities of the body tissues (e.g., muscle contraction and bone displacement) from the skin deformation, we need to create a database of the activities and the deformation. If we can measure the skin deformation by using the sensor array and an image of the cross-section of the forearm or upper arm by using an MRI at the same time, we can make the database. By using the MRI, we can also get the displacement of the bones. By using the database and some machine learning techniques, there is a possibility to estimate the activities of the body tissues from the skin deformation.

Chapter 7

Conclusion

7.1 Summary

In this dissertation, we proposed upper limb motion estimation methods based on skin deformation. We developed the distance sensor arrays to measure the skin deformation on the forearm and upper arm. To apply the methods to various applications, we developed two categories of motion estimation. In the first category, we developed a motion recognition method based on forearm deformation. The recognition method classified seven different types of motions including the motions caused by the activities of deep layer muscles. In the second category, we developed two pose estimation methods. One method used the forearm deformation and the other used the upper arm deformation. These pose estimation methods estimated multiple joint angles of the upper limb.

Generally, our proposed method was accurately able to estimate the aspects related to the activities of the deep layer muscles. This is an advantage of our method compared to other studies of the motion estimation based on sEMG. Moreover, unlike FMG-based methods, our method does not need to provide the fixture of the sensor whose shape is closely matched to the forearm, because our distance sensor array is fitted to the user's forearm by the sponge. From the results of chapter 3 to chapter 5, the skin deformation measured with the developed distance sensor arrays showed better performance and usefulness for the upper limb motion estimation.

In chapter 2, we designed the arrays to accurately measure skin deformation as displacements on several points on the skin surface. By the size-adjustment mechanism, the arrays could be applied to a variety of the size of the forearm and upper arm. The signals of the arrays could be measured without any amplifier or filters. Moreover, the arrays could measure skin deformation over the clothing.

In chapter 3, we confirmed that our proposed method could accurately recognize seven different types of hand motions including the motions related to the

activities of the deep layer muscles. The developed sensor array could measure the forearm deformation at the position close to the elbow where various muscles are located. Comparing to other studies that also used distance sensor arrays which measured deformation of the wrist, the back of the hand, or the longitudinal direction on the forearm, our method could obtain more information and recognize more hand motions from the activities of the deep layer muscles. Also, we confirmed that using training data of various elbow postures, the proposed method could recognize hand motions with different elbow postures. This result supports that the proposed method can be used without restricting motions of other body parts of the user. Also, we experimentally showed that this method could accurately recognize hand motions both with direct measurement and measurement over the clothing. This is a useful ability for the input interfaces of prosthetic hands or robotic exoskeletons since some users like to wear clothing when using a prosthetic hand or robotic exoskeleton.

In chapter 4, we confirmed that our proposed method was able to estimate multiple joint angles of the upper limb based on the forearm deformation. From the results of the experiments, forearm deformation shows the better performance of the upper limb motion estimation in not only single-axis motions but also daily life motions. In experiments where hand joint angles and upper limb poses are estimated, the forearm deformation still showed a good performance to estimate motions related to the activities of the deep layer muscles. The method could also estimate elbow joint angles; we regard the characteristic that elbow motion also deforms a forearm not as a nuisance rather as useful information. Our method uses only the wearable device which is attached to the forearm position close to the elbow. From our best knowledge, the study of the pose estimation at the multiple joint angles including the forearm, hand, and fingers based on bio-signal of the forearm position close to the elbow is nothing. Thus, our method showed a possibility to expand the application of the methods based on the bio-signals.

In chapter 5, we also confirmed that the upper arm deformation enabled the forearm pose estimation. Our method was able to estimate joint angles of elbow flexion and extension and forearm pronation and supination at the same time with combined motions. Our method could estimate the forearm poses only from the upper arm (not forearm) deformation. That provides the variation of the

sensor attached position for the various application.

In chapter 6, we analyzed the relationship between the skin deformation and the sEMG. The differences are measurement conditions, target tissues, and acquired signals. In particular, the advantage of the skin deformation is that it could provide not only the activities of the muscles but also the displacement of the bones and tendons. We also discussed the potential applications of the methods. By realizing additional things by each application, the methods will apply various fields.

In short, from high performance with all of the methods, we confirmed that measurement of skin deformation using the distance sensor array produces data containing information for estimation of upper limb motion. Thus, we verified that the potential of the skin deformation for the input source of information for the upper limb motion estimation.

7.2 Future Work

In the future, we will try to apply the methods to various applications. The target motions and the number of the sensors which can be attached to the body may be different by each application. As the number of sensors decreases, the number of motion types/joints to be estimated tends to be reduced. But the measurement system is rather miniaturized and simplified. Moreover, skin deformation may provide information of not only pose but also force. We experimentally confirmed the possibility of the estimation for both pose and force [64]. So, we will also try to estimate not only the upper limb pose but also joint torque. In addition, we will try to apply the skin deformation for the bio-mechanical analysis.

Publication list

Refereed Journal Papers

1. **Sung-Gwi Cho**, Masahiro Yoshikawa, Ming Ding, Jun Takamatsu, and Tsukasa Ogasawara, “Machine-learning-based Hand Motion Recognition System by Measuring Forearm Deformation with a Distance Sensor Array,” *International Journal of Intelligent Robotics and Applications*, vol. 3, no. 4, pp. 418–429, Nov, 2019.

Refereed International Conference Proceedings Papers

1. **Sung-Gwi Cho**, Kurasumi Tetsuya, Masahiro Yoshikawa, Ming Ding, Jun Takamatsu, and Tsukasa Ogasawara, “Estimation of Forearm Pose Based on Upper Arm Deformation Using a Deep Neural Network,” in Proceedings of *the IEEE International Conference on Robotics and Biomimetics (ROBIO2019)*, pp. 1246-1251, Dali, China, Dec, 2019.
2. **Sung-Gwi Cho**, Masahiro Yoshikawa, Ming Ding, Jun Takamatsu, and Tsukasa Ogasawara, “Estimation of Hand Motion Based on Forearm Deformation,” in Proceedings of *the IEEE International Conference on Robotics and Biomimetics (ROBIO2018)*, pp. 2291-2296, Kuala Lumpur, Malaysia, Dec, 2018
3. **Sung-Gwi Cho**, Masahiro Yoshikawa, Ming Ding, Jun Takamatsu, and Tsukasa Ogasawara, “Hand Motion Recognition Using a Distance Sensor Array,” in Proceedings of *the IEEE International Symposium on Robot and Human Interactive Communication (RO-MAN2017)*, pp. 1459-1484, Lisbon, Portugal, Aug, 2017.

Domestic Conference Proceedings Papers

1. 趙 崇貴, 倉角 哲也, 吉川 雅博, 丁 明, 高松 淳, 小笠原 司, “深層学習を用いた上腕形状変化に基づく肘と前腕の関節角度推定,” 第37回日本ロボット学会学術講演会 (RSJ2019), 1N2-02, 早稲田, 9月, 2019.
2. 趙 崇貴, 吉川 雅博, 丁 明, 高松 淳, 小笠原 司, “距離センサアレイを用いた上腕形状計測に基づく肘関節角度の推定,” 第36回日本ロボット学会学術講演会 (RSJ2018), 3A1-05, 春日井, 9月, 2018.
3. 趙 崇貴, 清川 拓哉, 友近 圭汰, 吉川 雅博, 小笠原 司, “前腕形状計測に基づく手の動作認識によるロボットアームの操作,” ヒューマンインタフェースシンポジウム 2017, 7D2-2, 大阪, 9月, 2017.
4. 趙 崇貴, 吉川 雅博, 丁 明, 高松 淳, 小笠原 司, “距離センサアレイを用いた前腕形状計測に基づく手の関節角度の推定,” ロボティクス・メカトロニクス講演会 2017 (ROBOMECH2017), 2P2-M07, 郡山, 5月, 2017.

References

- [1] D. Rakita, B. Mutlu, and M. Gleicher, “A motion retargeting method for effective mimicry-based teleoperation of robot arms,” in Proceedings of *the ACM/IEEE International Conference on Human-Robot Interaction (HRI)*, pp. 361–370, 2017.
- [2] C. Cipriani, F. Zaccone, S. Micera, and M. C. Carrozza, “On the shared control of an emg-controlled prosthetic hand: analysis of user–prosthesis interaction,” *IEEE Transactions on Robotics*, vol. 24, no. 1, pp. 170–184, 2008.
- [3] N. S. K. Ho, K. Y. Tong, X. L. Hu, K. L. Fung, X. J. Wei, W. Rong, and E. A. Susanto, “An emg-driven exoskeleton hand robotic training device on chronic stroke subjects: Task training system for stroke rehabilitation,” in Proceedings of *the IEEE International Conference on Rehabilitation Robotics (ICORR)*, pp. 1–5, June 2011.
- [4] D. Leonardis, M. Barsotti, C. Loconsole, M. Solazzi, M. Troncossi, C. Mazzotti, V. P. Castelli, C. Procopio, G. Lamola, C. Chisari, M. Bergamasco, and A. Frisoli, “An emg-controlled robotic hand exoskeleton for bilateral rehabilitation,” *IEEE Transactions on Haptics*, vol. 8, no. 2, pp. 140–151, 2015.
- [5] A. Atasoy, E. Kaya, E. Toptas, S. Kuchimov, E. Kaplanoglu, and M. Ozkan, “24 dof EMG controlled hybrid actuated prosthetic hand,” in Proceedings of *the Annual International Conference of the IEEE Engineering in Medicine and Biology Society (EMBC)*, pp. 5059–5062, 2016.
- [6] C. Meeker, S. Park, L. Bishop, J. Stein, and M. Ciocarlie, “EMG pattern classification to control a hand orthosis for functional grasp assistance after stroke,” in Proceedings of *the IEEE international conference on rehabilitation robotics (ICORR)*, pp. 1203–1210, 2017.
- [7] Y. Yun, S. Dancausse, P. Esmatloo, A. Serrato, C. A. Merring, P. Agarwal, and A. D. Deshpande, “Maestro: an EMG-driven assistive hand exoskeleton

- for spinal cord injury patients,” in Proceedings of *the IEEE International Conference on Robotics and Automation (ICRA)*, pp. 2904–2910, 2017.
- [8] B. Ploderer, J. Fong, A. Withana, M. Klačic, S. Nair, V. Crocher, F. Vetere, and S. Nanayakkara, “Armsleeve: a patient monitoring system to support occupational therapists in stroke rehabilitation,” in Proceedings of *the ACM Conference on Designing Interactive Systems*, pp. 700–711, 2016.
- [9] S. Fantozzi, A. Giovanardi, F. A. Magalhães, R. Di Michele, M. Cortesi, and G. Gatta, “Assessment of three-dimensional joint kinematics of the upper limb during simulated swimming using wearable inertial-magnetic measurement units,” *Journal of Sports Sciences*, vol. 34, no. 11, pp. 1073–1080, 2016.
- [10] T. Stiefmeier, D. Roggen, G. Ogris, P. Lukowicz, and G. Tröster, “Wearable activity tracking in car manufacturing,” *IEEE Pervasive Computing*, vol. 7, no. 2, pp. 42–50, 2008.
- [11] C. Bi, J. Huang, G. Xing, L. Jiang, X. Liu, and M. Chen, “Safewatch: A wearable hand motion tracking system for improving driving safety,” in Proceedings of *the 2017 IEEE/ACM Second International Conference on Internet-of-Things Design and Implementation (IoTDI)*, pp. 223–232, 2017.
- [12] C. Zhu and W. Sheng, “Wearable sensor-based hand gesture and daily activity recognition for robot-assisted living,” *IEEE Transactions on Systems, Man, and Cybernetics-Part A: Systems and Humans*, vol. 41, no. 3, pp. 569–573, 2011.
- [13] T. Simon, H. Joo, I. Matthews, and Y. Sheikh, “Hand keypoint detection in single images using multiview bootstrapping,” in Proceedings of *the IEEE Conference on Computer Vision and Pattern Recognition (CVPR)*, pp. 1145–1153, 2017.
- [14] Y. Cai, L. Ge, J. Cai, and J. Yuan, “Weakly-supervised 3d hand pose estimation from monocular rgb images,” in Proceedings of *the European Conference on Computer Vision (ECCV)*, pp. 666–682, 2018.

- [15] S. Sridhar, A. Oulasvirta, and C. Theobalt, “Interactive markerless articulated hand motion tracking using rgb and depth data,” in Proceedings of *the IEEE international conference on computer vision (ICCV)*, pp. 2456–2463, 2013.
- [16] Z. Ren, J. Yuan, J. Meng, and Z. Zhang, “Robust part-based hand gesture recognition using kinect sensor,” *IEEE Transactions on Multimedia*, vol. 15, no. 5, pp. 1110–1120, 2013.
- [17] H.-S. Yeo, E. Wu, J. Lee, A. Quigley, and H. Koike, “Opisthenar: Hand poses and finger tapping recognition by observing back of hand using embedded wrist camera,” in Proceedings of *the Annual ACM Symposium on User Interface Software and Technology*, pp. 963–971, 2019.
- [18] Y. Lecun, L. Bottou, Y. Bengio, P. Haffner *et al.*, “Gradient-based learning applied to document recognition,” *Proceedings of the IEEE*, vol. 86, no. 11, pp. 2278–2324, 1998.
- [19] L. Ge, H. Liang, J. Yuan, and D. Thalmann, “Robust 3d hand pose estimation in single depth images: from single-view cnn to multi-view cnns,” in Proceedings of *the IEEE Conference on computer vision and pattern recognition (CVPR)*, pp. 3593–3601, 2016.
- [20] O. Koller, H. Ney, and R. Bowden, “Deep hand: How to train a cnn on 1 million hand images when your data is continuous and weakly labelled,” in Proceedings of *the IEEE Conference on Computer Vision and Pattern Recognition (CVPR)*, pp. 3793–3802, 2016.
- [21] H. G. Kortier, V. I. Sluiter, D. Roetenberg, and P. H. Veltink, “Assessment of hand kinematics using inertial and magnetic sensors,” *Journal of Neuro-Engineering and Rehabilitation*, vol. 11, no. 1, pp. 70–83, 2014.
- [22] H. G. Kortier, J. Antonsson, H. M. Schepers, F. Gustafsson, and P. H. Veltink, “Hand pose estimation by fusion of inertial and magnetic sensing aided by a permanent magnet,” *IEEE Transactions on Neural Systems and Rehabilitation Engineering*, vol. 23, no. 5, pp. 796–806, 2015.

- [23] B. Fang, F. Sun, H. Liu, and C. Liu, “3d human gesture capturing and recognition by the immu-based data glove,” *Neurocomputing*, vol. 277, pp. 198–207, 2018.
- [24] P. Rivera, E. Valarezo, and T.-S. Kim, “Recognition of human hand activities based on a single wrist imu using recurrent neural networks,” *International Journal of Pharma Medicine and Biological Sciences*, pp. 114–118, 2017.
- [25] Y.-H. Lee, M. Kim, H.-Y. Kim, D. Lee, and B.-J. You, “Chicap: low-cost hand motion capture device using 3d magnetic sensors for manipulation of virtual objects,” in Proceedings of *the ACM SIGGRAPH 2018 Emerging Technologies*, pp. 1–2, 2018.
- [26] P. Kieliba, P. H. Veltink, T. L. Baldi, D. Prattichizzo, G. Santaera, A. Bicchi, M. Bianchi, and B.-J. F. Van Beijnum, “Comparison of three hand pose reconstruction algorithms using inertial and magnetic measurement units,” in Proceedings of *the IEEE-RAS International Conference on Humanoid Robots (Humanoids)*, pp. 1–9, 2018.
- [27] M. Yoshikawa, M. Mikawa, and K. Tanaka, “A myoelectric interface for robotic hand control using support vector machine,” in Proceedings of *the IEEE/RSJ International Conference on Intelligent Robots and Systems (IROS)*, pp. 2723–2728, 2007.
- [28] K. Shima and T. Tsuji, “Classification of combined motions in human joints through learning of individual motions based on muscle synergy theory,” in Proceedings of *the IEEE/SICE International Symposium on System Integration (SII)*, pp. 323–328, 2010.
- [29] W. Guo, X. Sheng, J. Liu, L. Hua, D. Zhang, and X. Zhu, “Towards zero training for myoelectric control based on a wearable wireless semg armband,” in Proceedings of *the IEEE International Conference on Advanced Intelligent Mechatronics (AIM)*, pp. 196–201, 2015.
- [30] A. A. Adewuyi, L. J. Hargrove, and T. A. Kuiken, “An analysis of intrinsic and extrinsic hand muscle emg for improved pattern recognition con-

- trol,” *IEEE Transactions on Neural Systems and Rehabilitation Engineering*, vol. 24, no. 4, pp. 485–494, 2016.
- [31] L. Pan, D. L. Crouch, and H. H. Huang, “Comparing EMG-based human-machine interfaces for estimating continuous, coordinated movements,” *IEEE Transactions on Neural Systems and Rehabilitation Engineering*, 2019.
- [32] F. Xiao, Y. Wang, L. He, H. Wang, W. Li, and Z. Liu, “Motion estimation from surface electromyogram using adaboost regression and average feature values,” *IEEE Access*, vol. 7, pp. 13 121–13 134, 2019.
- [33] Q. Ding, X. Zhao, A. Xiong, and J. Han, “A novel motion estimate method of human joint with emg-driven model,” in Proceedings of *the IEEE International Conference on Bioinformatics and Biomedical Engineering*, pp. 1–5, 2011.
- [34] Y. Chen, X. Zhao, and J. Han, “Hierarchical projection regression for online estimation of elbow joint angle using emg signals,” *Neural Computing and Applications*, vol. 23, no. 3-4, pp. 1129–1138, 2013.
- [35] Z. G. Xiao and C. Menon, “Performance of forearm fmg and semg for estimating elbow, forearm and wrist positions,” *Journal of Bionic Engineering*, vol. 14, no. 2, pp. 284–295, 2017.
- [36] A. Radmand, E. Scheme, and K. Englehart, “High-density force myography: A possible alternative for upper-limb prosthetic control,” *Journal of Rehabilitation Research & Development*, vol. 53, no. 4, pp. 443–457, 2016.
- [37] N. Li, S. Wei, M. Wei, B. Liu, H. Huo, and L. Jiang, “Hand motion recognition based on pressure distribution maps and ls-svm,” in Proceedings of *the IEEE International Conference on Mechatronics and Control (ICMC)*, pp. 1027–1031, 2014.
- [38] A. Dementyev and J. A. Paradiso, “Wristflex: low-power gesture input with wrist-worn pressure sensors,” in Proceedings of *the ACM Annual Symposium on User interface software and technology (UIST)*, pp. 161–166, 2014.

- [39] P.-G. Jung, G. Lim, S. Kim, and K. Kong, “A wearable gesture recognition device for detecting muscular activities based on air-pressure sensors,” *IEEE Transactions on Industrial Informatics*, vol. 11, no. 2, pp. 485–494, 2015.
- [40] Y. Kamei and S. Okada, “Classification of forearm and finger motions using electromyogram and arm-shape-changes,” in Proceedings of *the IEEE Annual International Conference of the Engineering in Medicine and Biology Society (EMBC)*, pp. 5680–5683, 2016.
- [41] N. Akhlaghi, C. A. Baker, M. Lahlou, H. Zafar, K. G. Murthy, H. S. Rangwala, J. Kosecka, W. M. Joiner, J. J. Pancrazio, and S. Sikdar, “Real-time classification of hand motions using ultrasound imaging of forearm muscles,” *IEEE Transactions on Biomedical Engineering*, vol. 63, no. 8, pp. 1687–1698, 2015.
- [42] Y. Irvantchi, M. Goel, and C. Harrison, “Beamband: Hand gesture sensing with ultrasonic beamforming,” in Proceedings of *the 2019 CHI Conference on Human Factors in Computing Systems*, pp. 1–10, 2019.
- [43] H. Kato and K. Takemura, “Hand pose estimation based on active bone-conducted sound sensing,” in Proceedings of *the 2016 International Joint Conference on Pervasive and Ubiquitous Computing: Adjunct*, pp. 109–112, 2016.
- [44] Y. Makino, Y. Sugiura, M. Ogata, and M. Inami, “Tangential force sensing system on forearm,” in Proceedings of *the Augmented Human International Conference*, pp. 29–34, 2013.
- [45] M. Ogata and M. Imai, “Skinwatch: skin gesture interaction for smart watch,” in Proceedings of *the Augmented Human International Conference*, pp. 21–24, 2015.
- [46] H. Oka, Y. Konishi, T. Kitawaki, N. Ichihashi, and M. Yoshida, “Development of multichannel array transducer of displacement mechanical-myogram,” in Proceedings of *the Annual International Conference of the IEEE Engineering in Medicine and Biology Society (EMBC)*, pp. 5899–5902, 2013.

- [47] R. Fukui, M. Watanabe, M. Shimosaka, and T. Sato, “Hand shape classification in various pronation angles using a wearable wrist contour sensor,” *Advanced Robotics*, vol. 29, no. 1, pp. 3–11, 2015.
- [48] Y. Sugiura, F. Nakamura, W. Kawai, T. Kikuchi, and M. Sugimoto, “Behind the palm: Hand gesture recognition through measuring skin deformation on back of hand by using optical sensors,” in Proceedings of *the Annual Conference of the Society of Instrument and Control Engineers of Japan (SICE)*, pp. 1082–1087, 2017.
- [49] A. Kato, Y. Matsumoto, Y. Kobayashi, S. Sugano, and M. G. Fujie, “Estimating a joint angle by means of muscle bulge movement along longitudinal direction of the forearm,” in Proceedings of *the IEEE International Conference on Robotics and Biomimetics (ROBIO)*, pp. 614–619, 2015.
- [50] M. Yoshikawa, Y. Taguchi, S. Sakamoto, S. Yamanaka, Y. Matsumoto, T. Ogasawara, and N. Kawashima, “Trans-radial prosthesis with three opposed fingers,” in Proceedings of *the IEEE/RSJ International Conference on Intelligent Robots and Systems (IROS)*, pp. 1493–1498, 2013.
- [51] T. Cover and P. Hart, “Nearest neighbor pattern classification,” *IEEE Transactions on Information Theory*, vol. 13, no. 1, pp. 21–27, January 1967.
- [52] B. E. Boser, I. M. Guyon, and V. N. Vapnik, “A training algorithm for optimal margin classifiers,” in Proceedings of *the ACM Annual Workshop on Computational learning theory (COLT)*, pp. 144–152, 1992.
- [53] Y. Bengio *et al.*, “Learning deep architectures for ai,” *Foundations and trends® in Machine Learning*, vol. 2, no. 1, pp. 1–127, 2009.
- [54] D. P. Kingma and J. Ba, “Adam: A method for stochastic optimization,” *arXiv preprint arXiv:1412.6980*, 2014.
- [55] V. Vapnik, S. E. Golowich, and A. J. Smola, “Support vector method for function approximation, regression estimation and signal processing,” in Proceedings of *the Advances in neural information processing systems (NIPS)*, pp. 281–287, 1997.

- [56] “Leap motion,” <https://www.leapmotion.com/>.
- [57] “Perception neuron,” <https://neuronmocap.com/>.
- [58] J. G. Ngeo, T. Tamei, and T. Shibata, “Continuous and simultaneous estimation of finger kinematics using inputs from an emg-to-muscle activation model,” *Journal of neuroengineering and rehabilitation*, vol. 11, no. 122, pp. 1–14, 2014.
- [59] F. Quivira, T. Koike-Akino, Y. Wang, and D. Erdogmus, “Translating semg signals to continuous hand poses using recurrent neural networks,” in *Proceedings of the IEEE EMBS International Conference on Biomedical and Health Informatics (BHI)*, pp. 166–169, 2018.
- [60] C. L. Pulliam, J. M. Lambrecht, and R. F. Kirsch, “Emg-based neural network control of transhumeral prostheses,” *Journal of rehabilitation research and development*, vol. 48, no. 6, pp. 739–754, 2011.
- [61] Y. Kawai and H. Harashima, *NIKUTAN*. NTS Inc., 2004.
- [62] T. Sato, Y. Konishi, M. Naganuma, K. Suzuki, A. Narita, H. Fujii, W. Hashizume, and A. Naito, “Effects of wrist flexion and extension on forearm pronation force,” *Structure and Function*, vol. 9, no. 2, pp. 59–63, 2011.
- [63] R. Sagawa, K. Ayusawa, Y. Yoshiyasu, and A. Murai, “Predicting muscle activity and joint angle from skin shape,” in *Proceedings of the European Conference on Computer Vision (ECCV)*, pp. 488–502, 2018.
- [64] T. Kurasumi, S.-G. Cho, M. Ding, G. A. Garcia Ricardez, J. Takamatsu, and T. Ogasawara, “Simultaneous estimation of elbow joint angle and load based on upper arm deformation,” in *Proceedings of the IEEE International Conference on Cyborg and Bionic Systems (CBS)*, pp. 136–141, 2019.

Acknowledgements

First of all, I would like to thank my professor and dissertation adviser, Professor Tsukasa Ogasawara. He has welcomed me to the Robotics Laboratory and helped me. His nurturing ways of managing my research have helped me a lot in growing as a researcher and as a person. With his guidance generosity, I was able to accomplish this dissertation. Without him, this dissertation would not be possible.

I would like to thank my dissertation advisers, Associate Professor Jun Takamatsu and Visiting Assistant Professor Ming Ding. They pushed me to greater heights and gave me much needed advice on how to go about my research. Their forthright and discerning guidance steered me in the right direction and helped me clear the path towards the completion of this dissertation.

A special thanks to my other dissertation adviser, Associate Professor Masahiro Yoshikawa of Osaka Institute of Technology. He helped my research from the beginning when I was a master student. He always gave me a lot of advice for my research. Without advice from his objective perspective, this dissertation could not be accomplished.

Besides my advisers, I would also like to thank the rest of my dissertation committee: Professor Yoshinobu Satou. Thank you very much for reviewing my dissertation and invaluable guidance.

I would also like to thank the Human Modeling Group members of the Robotics Laboratory, especially Takaya Higuchi, Shori Kinoshita, Tetsuya Kurasumi, Mikihisa Nagashima, Tomoko Yui, and Tomoki Ishikura. They always help me not only research but also daily life.

I would also like to thank all the members of the Robotics Laboratory, past and present. Special mention to Gustavo Alfonso Garcia Ricardez, Lotfi El Hafi, Felix Wolf Hans Erich von Drigalski, Satoki Tsuichihara, Yuya Hakamata, Wataru Yamazaki, Pedro Miguel Uriguen Eljuri, Takuya Kiyokawa, and Naoki Shirakura.

Let me also thank the administrative staffs in the Lab. who have been patient with me and helped me with the bureaucratic side of being a student: Michiyo Owaki and Miki Ikeda.

I would like to thank all my friends here for joining me in my life trav-

els throughout. In particular, my colleagues who had been always together in my master's course of NAIST, Tomoyuki Taguchi, Daisuke Kakuma, Atsushi Ito, Yosuke Osaki, Tetsuya Onaka, Shohki Kanda, Ryuzo Baba, Yukiya Fukui, Takumi Fujiyama, Ryota Matsuura, and Akishige Yuguchi.

Moreover, I would like to thank the society of Korean in Japan. They helped and gave me a lot of encouragement at any time. With their kindness and support, I could continue my research in Japan and the world.

Finally, I would like to conclude this dissertation with deeply grateful thanks to my parents and two older brothers for supporting me at any time.